Delft University of Technology

MSc Thesis Report

# Development and Assessment of Resource Management Solutions for Throughput Enhancement in a RIS-aided Mobile Network

*Author:*
Sakshi Agarwal (5456029)
*Thesis committee:*

Dr. Geethu Joseph
Assistant professor,
TU Delft

Dr. Remco Litjens
Associate Professor,
TU Delft
Senior scientist, TNO

Dr. Kallol Das
Senior scientist, TNO

August 29, 2023

TU Delft

TNO innovation for life

# Preface

I'm pleased to present this thesis as the final requirement for a Master's degree in Electrical Engineering at Delft University of Technology, specializing in Wireless Communications and Sensing. This endeavor has been a remarkable path of growth, learning, and collaboration, shaped by the support and contributions of numerous individuals and institutions.

Foremost, I extend deep gratitude to Dr. Remco Litjens, my core supervisor, and Dr. Kallol Das, my company supervisor. Their steadfast guidance, expertise, and encouragement have profoundly influenced this research's trajectory. Dr. Litjens initiated my involvement through an internship at TNO, a pivotal experience that established the thesis's research problem. Their ongoing feedback and motivation have been instrumental in steering this work to fruition.

I also acknowledge Dr. Geethu Joseph for her active participation in numerous thesis meetings, enriching discussions, and outcomes.

This research was conducted at The Netherlands Organisation for Applied Scientific Research (TNO) in The Hague. My appreciation extends to TNO for fostering an environment conducive to research and learning, and for the collaborative opportunities between TU Delft and TNO that have enriched my academic journey.

To my colleagues, friends, and fellow researchers, I extend heartfelt gratitude for intellectual exchanges, discussions, and shared experiences that broadened my horizons and deepened my understanding. This journey has had its challenges, and the companionship of friends has been a great source of solace.

Finally, I must acknowledge my family's unwavering support throughout this period. Their encouragement, patience, and belief in my capabilities have been my constant pillars of strength.

In conclusion, this thesis is a collective effort, a representation of collaborative efforts, dedication, and the pursuit of knowledge. As I present this work to the academic community, I hope it contributes to the field of mobile communications, enhancing future research opportunities.

Sakshi Agarwal

# Abstract

Reconfigurable Intelligent Surfaces (RIS) are envisioned to become a pivotal transformative technology within the realm of 6G mobile networks. In this study, we introduce three heuristic algorithms designed to optimize radio resource management, ultimately enhancing throughput within a RIS-enhanced mobile network. Our findings demonstrate that the algorithm which holistically optimizes user scheduling, RIS-UE association, cell precoding matrices, and RIS configuration matrices outperforms alternative strategies.

Moreover, our investigation delves into uncovering the most effective applications of RIS. This involves a thorough performance comparison of the algorithms across diverse scenarios, encompassing varying RIS deployment configurations (position and orientation), number of users in a network, and number of RIS elements. Additionally, we model the influence of blocker loss—characterized by blocker presence probability and strength—on throughput performance.

In the wake of our study, it becomes evident that RIS exhibits the most promising potential in scenarios involving MU-MIMO configurations, whether within single-cell or multi-cell layouts, and for both indoor and outdoor user settings. However, for SU-MIMO cases, RIS-induced throughput enhancement manifests exclusively in single-cell layouts, and particularly benefits outdoor users in environments marked by substantial blocker strength.

**Keywords: Reconfigurable Intelligent Surfaces (RIS), radio resource management, throughput enhancement, MIMO, SU-MIMO, MU-MIMO, cell-UE association, cell-RIS-UE association, user scheduling, beamforming, RIS optimization, 6G.**

# List of acronyms

| | |
|---|---|
| **3GPP** | 3rd Generation Partnership Project |
| **AE** | Antenna Element |
| **AI** | Artificial Intelligence |
| **AR** | Augmented Reality |
| **BL** | Blocker Loss |
| **BPL** | Building Penetration Loss |
| **BS** | Base Station |
| **CF** | Correction Factor |
| **CSI** | Channel State Information |
| **CQI** | Channel Quality Indicator |
| **DL** | Downlink |
| **eMBB** | Enhanced Mobile Broadband |
| **HD** | High Definition |
| **HBL** | Human Body Loss |
| **IoT** | Internet of Things |
| **KPI** | Key Performance Indicator |
| **LOS** | Line of Sight |
| **MCS** | Modulation and Coding Scheme |
| **MI** | Mutual Information |
| **MIESM** | Mutual Information Effective SINR Mapping |
| **MIMO** | Multiple-Input Multiple-Output |
| **ML** | Machine Learning |
| **MMTC** | Massive Machine-Type Communications |
| **MRC** | Maximal Ratio Combining |
| **MRT** | Maximum Ratio Transmission |
| **MU-MIMO** | Multi-User Multiple-Input Multiple-Output |
| **NOMA** | Non-Orthogonal Multiple Access |
| **PF** | Proportional Fairness |
| **PL** | Path Loss |
| **PRB** | Physical Resource Block |
| **QoS** | Quality of Service |
| **QuaDRiGa** | Quasi-Deterministic Radio channel Generator |
| **RAN** | Radio Access Network |
| **RIS** | Reconfigurable Intelligent Surface |

| | |
|---|---|
| **SDMA** | Spatial Division Multiple Access |
| **SINR** | Signal to Interference and Noise Ratio |
| **SMS** | Short Message Service |
| **SNR** | Signal-to-Noise Ratio |
| **SoA** | State of Art |
| **SRS** | Sounding Reference Signal |
| **SSB** | Synchronization Signal Blocks |
| **SU-MIMO** | Single-User Multiple-Input Multiple-Output |
| **SUS** | Semi-orthogonal User Selection |
| **TDD** | Time Division Duplexing |
| **TDMA** | Time Division Multiple Access |
| **TTI** | Transmission Time Interval |
| **UE** | User Equipment |
| **UL** | Uplink |
| **URLLC** | Ultra-Reliable Low-Latency Communications |
| **VR** | Virtual Reality |
| **ZF** | Zero Forcing |

# List of figures

# Table of contents

# Chapter 1

# Introduction

The continuous evolution of mobile networks from 1G to 5G has led to significant advancements, consistently pushing the boundaries of connectivity and transforming our modes of communication and interaction with the digital realm. This evolution is depicted in Figure 1.1. The first generation of wireless networks, 1G, was introduced in the 1980s using analog cellular technology for basic voice communication capabilities. It had limited capacity and voice quality. Subsequently, 2G brought digital communication, offering improved call quality and the ability to send text messages (SMS). It introduced more efficient utilization of the frequency spectrum compared to 1G. Within another decade, 3G networks emerged with faster data transfer rates, enabling services such as mobile internet access and video calling. This marked a significant shift towards data-centric services. By the late 2000s, 4G networks were introduced, bringing substantial improvements including significantly faster data speeds, reduced latency, and increased network capacity. This facilitated services like HD video streaming, online gaming, and advanced mobile applications.

Currently, we are in the phase of the 5G rollout. 5G employs higher frequency radio waves and advanced network architecture, including massive MIMO (Multiple Input, Multiple Output) and beamforming technologies. Furthermore, new concepts such as network virtualization and slicing enable faster data transfer rates, reduced signal interference, and more efficient use of available spectrum. This has resulted in supporting applications that require enhanced mobile broadband (eMBB), massive machine-type communications (MMTC), and ultra-reliable low-latency communications (URLLC).

Technology has come a long way from 1G to 5G, yet there are many milestones to achieve. Beyond 5G refers to the future generation of wireless communication technology that will succeed 5G networks. While still in early development, it aims to address the limitations of 5G and introduce even more advanced features. Technologies beyond 5G are expected to include higher frequencies, including terahertz (THz) communications, AI-driven networks (for smarter network management, optimization, and resource allocation), and quantum communications, among others. Beyond 5G is anticipated to bring forth innovative applications and enhance existing 5G applications, such as holographic communication, ultra-high-definition VR/AR, remote robotics, smart infrastructure, advanced healthcare, and

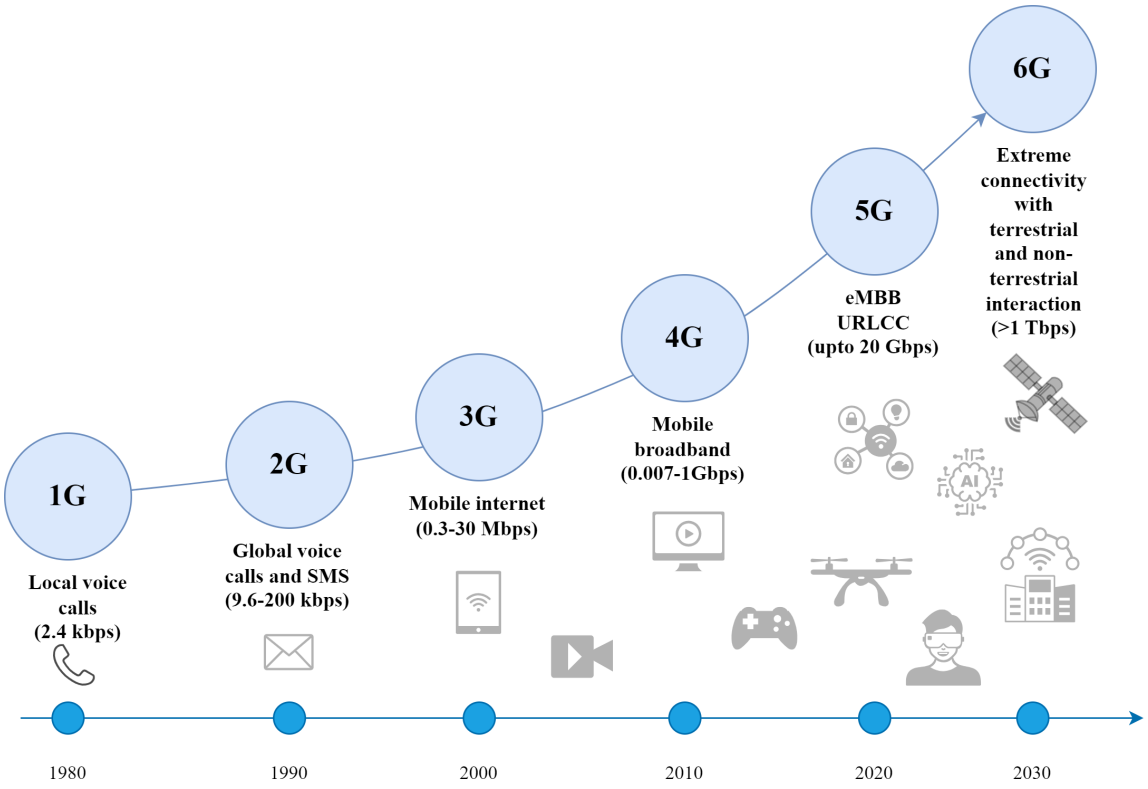


Figure 1.1: Evolution of mobile networks: 1G to 6G.

environmental monitoring.

6G, a conceptual framework for the future of wireless technology, represents the next step in achieving some of these milestones. Although still in its early stages, 6G envisions networks that offer even faster speeds, potentially reaching the terabits per second range. It is expected to support unprecedented levels of connectivity, enabling advanced applications like seamless human-machine interaction, advanced augmented reality, and highly sophisticated IoT systems.

To realize the ambitious vision of 6G, a range of key technologies are considered fundamental pillars of its infrastructure. Advanced antenna systems, leveraging innovative beamforming techniques, may enhance signal coverage, reliability, and capacity. Terahertz (THz) communication, operating at frequencies beyond 100 GHz, can facilitate unprecedented data rates and support the massive connectivity demands of the Internet of Things (IoT). The integration of satellite communication may extend the reach of 6G networks, ensuring seamless connectivity in remote and underserved areas.

Among these transformative technologies, the Reconfigurable Intelligent Surface (RIS) stands as a critical network component that could shape the future of 6G networks.

## 1.1 Reconfigurable Intelligent Surface (RIS)

RIS is a programmable array of tunable meta-surface elements capable of reflecting incoming signals in specific directions to create additional constructive paths alongside direct paths between the BS and a UE. Figure 1.2 illustrates how phases can be controlled using a phase shift circuit for each RIS element. RISs can be deployed flexibly, such as on walls or building sides, enabling received signals to be reflected towards users. RISs can enhance network performance, offer coverage in dead zones, or conserve energy. RISs are inherently passive, lacking active RF circuitry for signal reception or processing. By modifying the phase/amplitude of the reflected signal with low energy consumption, they create supplementary paths to receivers, improving link performance, and making RIS a promising candidate for 6G. "Reconfigurable" in RIS refers to the tunable elements, reconfigurable each time slot via a backhaul link. This enables RIS to create adaptable wireless channels that adjust to changing conditions, optimizing communication performance in real time.

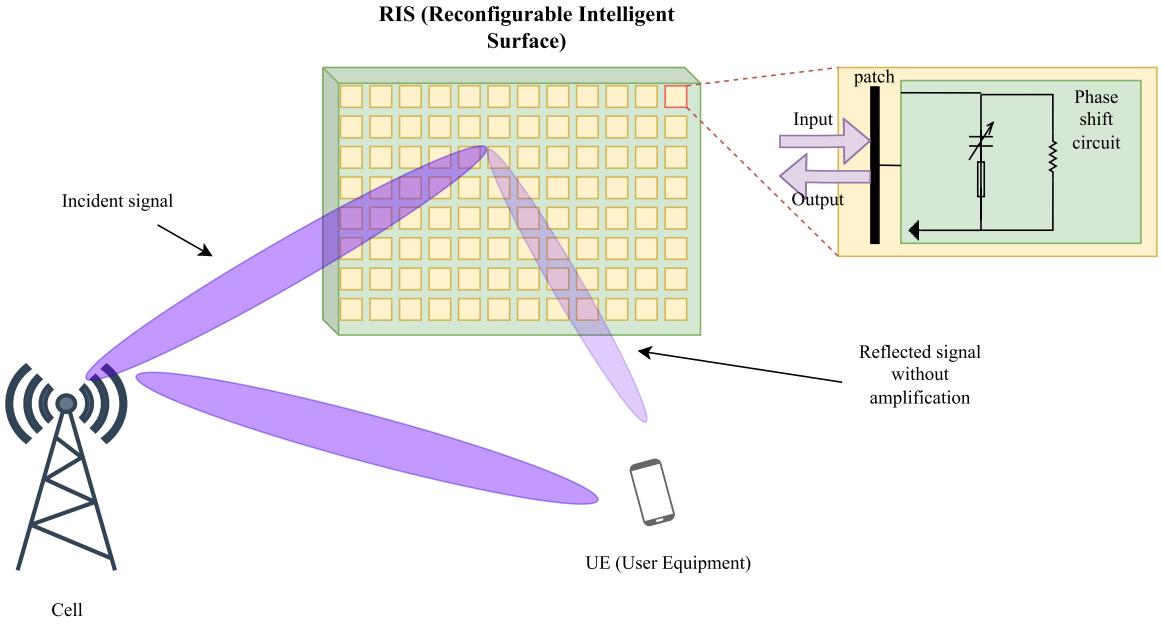


Figure 1.2: reflection via RIS.

RIS finds applications in a wide range of scenarios where wireless communication is essential. Some of these use cases are depicted in Figure 1.3. RIS can improve signal propagation in challenging indoor settings by strategically reflecting and redirecting signals to overcome obstacles, such as walls and furniture. In outdoor environments, RIS can enhance coverage and signal quality by intelligently reflecting signals to reach users in remote or obstructed areas. Researchers have observed performance gains when implementing RIS in different applications, including millimeter-wave (mmWave) non-orthogonal multiple access (NOMA) systems [3], vehicular systems [4], secure wireless communications [5], information and power transfer [6], and energy efficiency [7].

While RIS offers significant benefits and transformative potential for wireless communica-

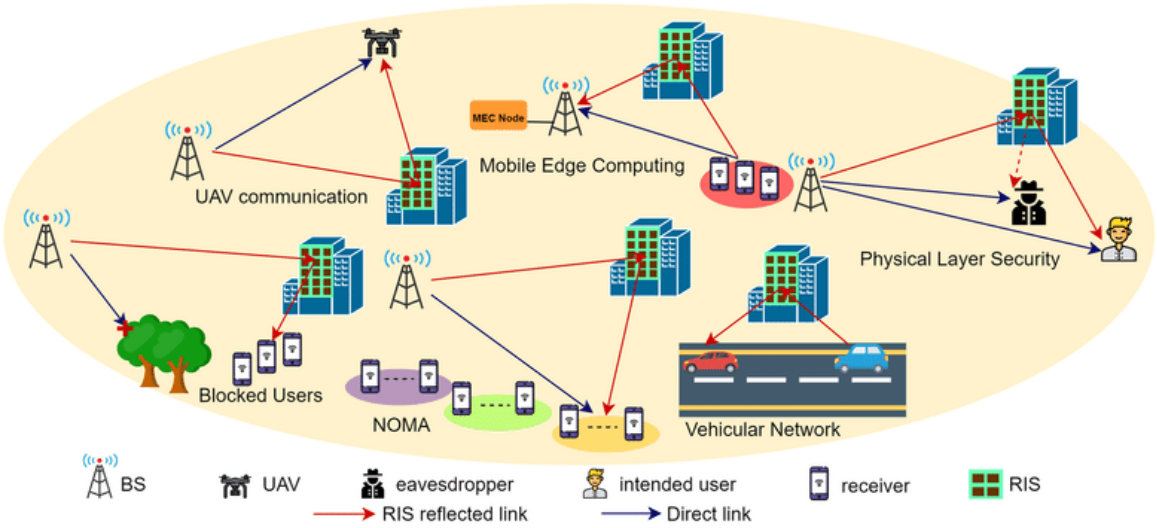


Figure 1.3: Applications of RIS. Adapted from [1].

tion systems, it also presents several challenges that need to be addressed for its successful deployment and realization of its full potential. These challenges include, but are not limited to:

- Design and Deployment: Designing and deploying large-scale RIS systems can be complex. Determining the optimal number and placement of reflecting elements, as well as their configuration and control mechanisms, requires careful consideration. The physical deployment of RIS in various environments, such as indoor spaces or outdoor areas, also poses challenges in terms of installation, calibration, and maintenance.

- Channel State Information (CSI) Acquisition: RIS relies on accurate and up-to-date information about the wireless channel for effective signal manipulation. However, acquiring precise channel state information becomes more challenging with the introduction of RIS.

- RIS Control and Management: Efficient control and management of RIS is crucial for its successful operation. Designing intelligent algorithms and protocols for dynamically configuring and adapting the behavior of RIS elements based on changing channel conditions and user requirements is a complex task. Developing efficient and scalable control mechanisms to handle a large number of reflecting elements and coordinate their actions is also a challenge.

In the past four years, RIS have garnered significant attention from researchers, resulting in extensive efforts to measure the performance gains of RIS in various applications and to tackle the challenges posed by this technology. Of particular interest to us is the challenge presented by **RIS deployment and RIS control and management**. In the following sections, we present a literature review conducted to address these two cases, aiming to identify the current state of the art and any existing gaps in the literature.

## 1.2 Literature review

While most papers consider a fixed arbitrary RIS deployment position, [8] offers a solution to the challenge of RIS deployment by optimizing the cell-RIS distance along with the RIS orientation for a single-cell single-user setup, aiming to maximize cell coverage. On the other hand, the authors of [9] compare two RIS deployment strategies: the distributed deployment of smaller RISs versus the centralized deployment of a larger RIS in the context of a single-cell two-user setup. Their findings demonstrate that the centrally located single RIS optimization yields better performance compared to strategically deployed multiple small RIS units. However, both these solutions overlook the complexities of a real-world multi-cell multi-user environment. RIS deployment considerations should encompass average cell loads, coverage dead zones, and the deployment environment (urban vs rural), areas that have yet to be addressed in the literature.

Moving on to address the challenge of RIS control and management, the literature presents a range of solutions. For instance, the joint optimization of beamforming precoders at the BS (active beamforming) and the RIS configuration matrix (passive beamforming) is proposed to minimize BS transmit power in a single-cell setup, catering to both single-user and multi-user scenarios. This optimization is achieved using semi-definite relaxation (SDR) and alternating optimization (AO) algorithms [10]. In contrast, other works employ fixed-point iteration and manifold optimization techniques to optimize active and passive beamforming for enhancing the signal strength in a single-cell single-user setup [11].

Given the computational intensity of RIS optimization, the literature has explored machine learning-based solutions. For instance, the authors of [12] utilize deep reinforcement learning to optimize the BS beamforming precoder and RIS configuration matrix, aiming to maximize the sum data rate in a single-cell multi-user MISO (multiple-input single-output) network. Similarly, Deep Neural Networks (DNN) are applied to optimize active and passive beamforming, with a focus on maximizing users' signal strength in scenarios where indoor signal quality is paramount [13].

It's important to note that the aforementioned studies primarily focus on single-cell setups and often overlook additional resource management tasks such as RIS-aware scheduling and BS-RIS-UE association. However, a limited body of literature explores AI-based solutions for optimizing various radio resource management tasks within a RIS-aided network. Notably, some authors leverage Graph Neural Networks (GNNs) to optimize RIS-aware user scheduling in conjunction with active and passive beamforming in a single-cell setup [14]. Additionally, a study considering a multi-cell MU-MIMO (multi-user multiple-input multiple-output) network is presented in [15], where authors optimize BS-RIS-UE associations alongside active and passive beamforming to maximize the sum data rate using deep reinforcement learning. However, this approach faces the challenge of stable BS-UE association over limited time slots. Furthermore, this approach assumes that all users are served at all times.

Through a comprehensive literature review, it becomes evident that while substantial contributions have been made in RIS control and management research, there is relatively less emphasis on RIS deployment strategies. Furthermore, the optimization of radio resource

management tasks, such as BS-RIS-UE association and user scheduling, remains underexplored within a realistic environment, particularly within traditional multi-cell MU-MIMO networks.

## 1.3 Objective

The objective of this thesis is **to optimize the radio resource management of a RIS-aided network for throughput enhancement**.

This thesis serves a dual purpose. Firstly, we employ two novel heuristic radio resource management algorithms with varying complexity to assess their impact on performance gains, specifically in terms of throughput, within a RIS-aided network. These algorithms are compared against a benchmark algorithm that represents radio resource management without utilizing the deployed RIS. Algorithm 1 focuses on optimizing RIS-UE associations and subsequently refining the RIS configuration matrix along with the BS precoding matrix after the user scheduling has been done for a given time slot. Algorithm 2 involves additionally RIS-aware scheduling, which in turn optimizes RIS-UE associations, the RIS configuration matrix, and the BS precoding matrix.

Secondly, our aim is to determine the most suitable use-case scenario for the RIS. We achieve this by evaluating the performance gains across various scenarios, such as single-cell versus multi-cell setups, single-user scheduling versus multi-user scheduling, indoor versus outdoor user placements, and in the presence of temporary blockers characterized by blocker strength and probability.

Ultimately, this thesis seeks to identify the optimal utilization scenario for RIS technology and to determine the algorithm that can extract the maximum benefit from the RIS in terms of throughput enhancement.

## 1.4 Thesis overview

With this objective in mind, we have structured the thesis into five distinct chapters.

In this introductory chapter, we provided the background and motivation behind the utilization RIS, highlighted the associated challenges, and outlined the central objective of the thesis.

Chapter 2 presents the overview of the traditional radio resource management tasks that accompany in a mobile network.

Chapter 3 offers an overview of the network modeling, including its components and the channel representation employed throughout the thesis.

Following the modeling discussion, Chapter 4 moves on to develop the research question, provided in this chapter, into a well-defined problem statement. Additionally, within this chapter, we delve into the intricacies of the three heuristic algorithms that we intend to utilize in solving the identified problem.

Subsequently, Chapter 5 introduces the metrics used to assess performance improvement and introduces various simulation scenarios. It then presents a comprehensive comparison of the outcomes yielded by the three algorithms across different scenarios.

The final chapter, Chapter 6, serves as the conclusion of this thesis. Here, we provide the core insights drawn from the study. We also outline the limitations of this research and suggest potential directions for future investigations.

For readers with a keen interest, Appendix A provides an exhaustive compilation of all results obtained across diverse scenarios during the course of the thesis.

The notations used in this paper are listed as follows. For any general matrix $\mathbf{H}$, $\mathbf{H}[i, j]$ denotes the entry at the $i^{th}$ row and the $j^{th}$ column, and $\mathbf{H}[:, j]$ denotes the column vector at the $j^{th}$ column. $\mathbf{H}^T$, $\mathbf{H}^*$, $\mathbf{H}^{-1}$, $\mathbf{H}^+$ represent the transpose, conjugate transpose, inverse, and moore-penrose pseudo-inverse of matrix $\mathbf{H}$ , respectively. $\mathbf{H}(t)$ is the value of $\mathbf{H}$ at time $t$ . $\mathbf{h}_k$ is the $k^{th}$ column vector of $\mathbf{H}$. For any column vector $\mathbf{h}$ (all vectors in this paper are column vectors), $\mathbf{h}(i)$ is the $i^{th}$ element. $|x|$ denotes the absolute value of the complex number $x$ and $||\mathbf{h}||_2$ denotes L-2 norm of the vector $\mathbf{h}$.

# Chapter 2

# Overview of existing radio resource management

This chapter guides the reader in understanding the existing mechanisms of traditional radio resource management tasks typically present in a mobile network. In this thesis, we use the same mechanisms with a slight modification.

## 2.1 Cell-user association

Cell-user association refers to the process of determining which cellular base station (cell) a specific user equipment (UE) or mobile device should be connected to. In a cellular network, multiple cells are deployed to provide coverage over a geographical area. The cell-user association mechanism ensures efficient utilization of network resources, optimal signal quality, and fair distribution of communication services among users. Factors influencing cell-user association include signal strength, interference, Quality-of-Service (QoS) requirements, handover, and user mobility.

In a 5G mobile network, all cells transmit beams in a periodic manner, namely SSBs (synchronization signal blocks). A given UE $u$ listens to these SSBs from all the cells and attempts a handshake with the cell with which it receives the best power. If it doesn't receive sufficient power from any cell then the user is considered out of coverage area. Thus, given user $u$ is associated to a given cell $c$ if:

$$c^u = \arg\max_{c \in \mathcal{C}} P_{c,u}^{SSB} \tag{2.1}$$

and,

$$P_{c^u,u}^{SSB} > P_{th}^{SSB} \tag{2.2}$$

where $\mathcal{C}$ is a set of all cells, $P_{c,u}^{SSB}$ is the maximum received SSB power from cell $c$ to user $u$, and $P_{th}^{SSB}$ is the threshold power needed for a UE receiver.

## 2.2 Scheduling

Given multiple calls at a given time, there is a need for a time-frequency scheduler at the cell end. We assume all calls operate at full wideband. In that case, there is an option for time-based multiplexing and/or spatial multiplexing.

The goal of a scheduler is to optimize the utilization of the network resources while considering various factors like fairness, data rates, and Quality of Service (QoS) requirements.

### 2.2.1 Schedulers

There are several scheduling algorithms used in wireless networks, each with its own approach and objectives. Three common scheduling algorithms are Round Robin, Maximum Ratio Scheduling, and Proportional Fair Scheduling.

#### Round robin scheduler

Round Robin is a simple and straightforward scheduling algorithm. It allocates resources in a cyclic manner to users in a predefined order. Each user takes turns receiving resources in a sequential fashion, ensuring that all users get an equal share of resources over time. While Round Robin is fair in the sense that no user is consistently prioritized, it may not be efficient for scenarios where users have different channel conditions or data rate requirements. Round Robin can lead to under-utilization of resources for users with good channel conditions and over-utilization for users with poor conditions.

#### Maximal ratio scheduler

Maximum Ratio Scheduling is an algorithm that prioritizes users based on their channel conditions, specifically the signal-to-noise ratio (SNR). It allocates resources to users with the highest SNRs, as they have the best potential for achieving higher data rates and better communication quality. It is particularly effective when channel conditions vary widely among users, as it ensures efficient use of the available resources by prioritizing those with the best links.

#### Proportional fair scheduler

Proportional fair scheduling strikes a balance between maximizing system throughput and ensuring fairness among users. It allocates resources to users in a way that takes into account both their channel conditions and their historical resource allocations. Users with better channel conditions receive more resources, but the algorithm also considers the needs of users with poorer channel conditions to maintain fairness. Proportional fair scheduling aims to provide each user with a proportional share of resources relative to their channel quality, avoiding extreme disparities in data rates among users.

For a given user $u$, with estimated data rates $\tilde{R}_u(t)$ at time $t$, proportional fairness index, $PF_u$, can be calculated as:

$$PF_u = \frac{\tilde{R}_u(t)}{R_u^{av}(t-1)} \tag{2.3}$$

where, $R_u^{av}(t-1)$ is the average user rate till time $t$. A user with a maximum $PF$ is then scheduled in the given TTI.

In this thesis, we use the proportional fair scheduler to ensure fairness among user throughputs.

### 2.2.2 Multi-user scheduling

Scheduling in MU-MIMO communication systems involves the allocation of communication resources to multiple users simultaneously, taking advantage of the spatial diversity provided by multiple antennas at both the transmitter and the receiver. MU-MIMO scheduling aims to improve system throughput, enhance spectral efficiency, and provide fairness among users.

#### SUS algorithm

Semi-orthogonal user selection (SUS) algorithm is a way to implement multi-user scheduling [16]. After ranking the users in terms of priority index (for us it is proportional fairness index (PF)), it first schedules the first user. It then co-schedules the user with the next best PF index, if it satisfies the condition of orthogonality between channels. Satisfying this condition means that any new user is co-scheduled if and only if the correlation of the channel (of this new user) with the span of the channel matrix of the already scheduled users is less than a threshold value.

## 2.3 Beamforming

Precoding refers to a signal processing technique used to improve the efficiency and quality of data transmission in multi-antenna communication systems. It involves applying specific transformations to the data before transmission from the transmitting antennas to enhance the signal's reception at the receiving antennas. Precoding aims to exploit the spatial diversity offered by multiple antennas to mitigate interference, enhance signal strength, and improve overall system performance.

There are two primary types of precoding techniques: Maximum Ratio Transmission (MRT) and Zero Forcing (ZF).

### 2.3.1 Maximum ratio transmission

MRT is a precoding technique that aims to maximize the SNR at the receiving end. It scales the signal transmitted from each antenna by the ratio of the channel gains (including fading) at the receiver to the corresponding transmitting antennas. For a given user $u$, precoder $\mathbf{w}_u(t)$ at time $t$ is given by:

$$\mathbf{w}_u(t) = \frac{\mathbf{h}_u(t)^*}{||\mathbf{h}_u(t)||_2} \tag{2.4}$$

where, $\mathbf{h}_u(t)$ represents the wideband channel for a single-antenna user $u$ from its associated cell at time $t$.

MRT is particularly useful in SU-MIMO communication when the receiver has perfect channel state information (CSI) and there is no interference. MRT can effectively improve the received signal strength, resulting in enhanced data rates and reduced error rates. However, it does not consider interference or noise in its design, which can limit its performance in scenarios with interference.

### 2.3.2 Zero forcing

ZF is another precoding technique that aims to eliminate interference at the receiving antennas by designing the precoding matrix to ensure that the transmitted signal is orthogonal to interfering signals. In ZF, the precoding matrix is computed in such a way that the interference introduced by transmitting antennas is nullified at the receiving end. ZF is particularly effective in scenarios with interference, as it can suppress interference and improve signal quality. However, ZF can amplify noise, especially when the number of receiving antennas is greater than the number of transmitting antennas. A ZF precoder at cell $c$ for all its scheduled users, denoted here as $W_c(t)$ at time $t$ is calculated as:

$$W_c(t) = (H_c^T)^+ \tag{2.5}$$

where $H_c^T$ denotes the wideband channel matrix comprising of channel vectors from the cell $c$ to all the scheduled single-antenna users. ZF is especially useful in an MU-MIMO that may suffer from high intra-cell interference [17].

## 2.4 Combiner

A combiner is a crucial component used in the receiver system of a multi-antenna communication system. Its primary purpose is to combine the signals received from different antennas, effectively combining their strengths and exploiting the diversity provided by multiple antennas to improve the overall quality of the received signal.

MRC is the most common combiner technique that maximizes the SINR by adjusting the weighting of the received signals based on their channel gains. It assigns greater weight to signals with stronger channel gains and lower weight to signals with weaker channel gains. This technique is particularly effective in combating fading and improving signal quality.

In a SU-MIMO, MRC combiner, $\mathbf{v}_u(t)$ at time $t$ is calculated as:

$$\mathbf{v}_u(t) = (\mathbf{w}_u(t)\mathbf{H}_u(t))^+ \tag{2.6}$$

where, $\mathbf{w}_u(t)$ represents the precoder for user $u$ and $\mathbf{H}_u(t)$ represents the wideband channel between the cell to the user $u$ at time $t$.

# Chapter 3

# Modeling

This chapter covers the modeling of the network, key components such as antenna and RIS, and the radio propagation channel considered in this thesis.

## 3.1 Network modeling

We consider a network comprising $N_C$ cells and the set of cells is denoted as $\mathcal{C}$. Considering a dense urban deployment, an inter-site distance of 500m is considered in this work [18]; this results in a cell range of 333m. Each cell is assigned a 20 MHz TDD carrier in the 3.5 GHz band configured with a numerology 1 (i.e. 30 kHz sub-carrier spacing). This results in a TTI (transmission time interval) of 0.5ms, where a TTI denotes the duration of transmission on the radio link. Since twelve sub-carriers make up a physical resource block, each cell has $N_{PRB} = 50$ PRBs. The set of all PRBs is denoted as $\mathcal{F}$. The carrier is configured with a five-slot TDD frame duration, comprising four downlink slots and one uplink slot. The total transmit power per cell is $P_T = 120W$, which is divided evenly among all PRBs.

We consider two network layouts: a single-cell layout and a multi-cell layout, as shown in Figures 3.1 (a) and (b), respectively. Height of each BS $H_{BS}$ is fixed at 25m. The single-cell layout consists of one particular cell (i.e. $N_C = 1$) of a three-sectorized BS site with its azimuth as shown by the array in Figure 3.1 a). For the multi-cell layout, we consider $N_C = 19$ cells of three-sectorized BS sites, as depicted in Figure 3.1 (b). The innermost cell, highlighted in dark green, is our cell of interest, i.e., the performance is evaluated for all the users of this cell and the outermost twelve cells, highlighted in red, serve the sole purpose of creating realistic interference for the inner (light green and dark green) cells.

Next in this network, we consider $N_U$ users uniformly distributed over the (dark or light) green cells and the set of users is denoted as $\mathcal{U}$. We do not model the explicit presence of any users in the outermost red cells but, for ease of simulations, assume that these cells transmit at a configured fixed transmit power with an antenna diagram specified in Section 3.2. We assume that all users are at a fixed height of $H_{UE} = 1.5m$, and are locally mobile at pedestrian speed. Users are active with persistent full-buffer data flows in the downlink for the entire simulation duration. We vary the value of $N_U$ to see the impact of the number

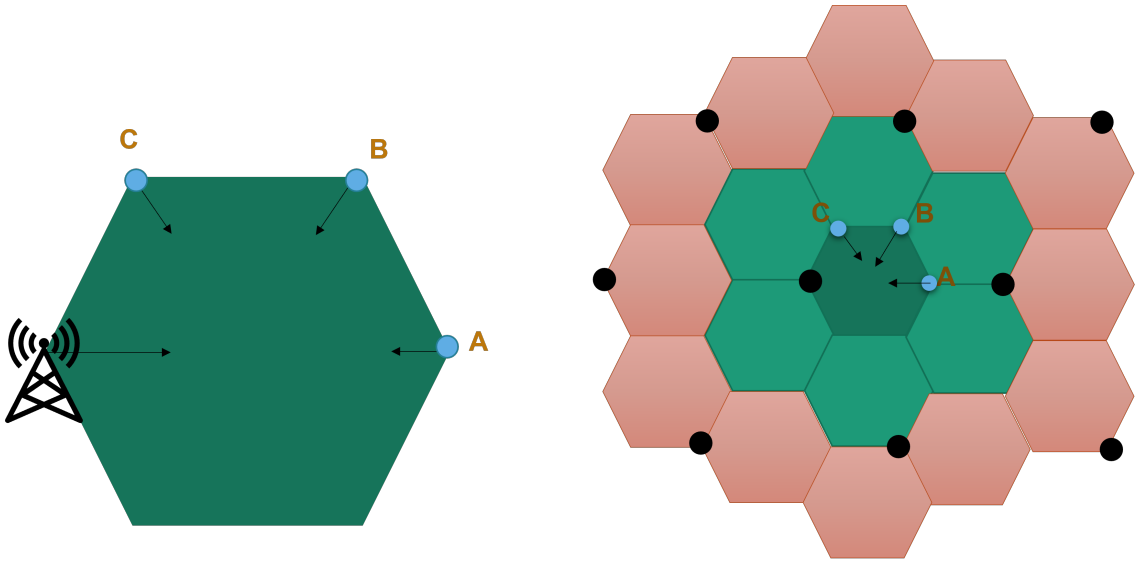


Figure 3.1: Network layouts for simulation consisting of a) a single-cell layout and b) a multi-cell layout, where each cell is part of a three-sectorized BS site. Users are uniformly distributed over the (dark or light) green cells. A single RIS is deployed at positions A, B, or C with their respectively indicated orientations.

of users in different scenarios and layouts. We consider two different cases, one having all users indoors and the other having all of the users outdoors to compare the performance of a RIS-aided network in both cases.

We are interested in recognizing the impact of RIS on radio resource management and the performance experienced by the users of the innermost cell. To investigate this, we consider one RIS in the network mounted on a building so that its center is at an assumed height of $H_{RIS} = 20m$. Three candidate RIS deployment positions are considered for both network layouts, represented by A, B, and C. These positions are selected as the three corners of the edge of the center cell. Each RIS deployment is characterized by its position and its azimuth direction.

## 3.2 Antenna modeling

Each cell is equipped with a 64T64R antenna array, comprising eight rows and four columns of cross-polarized antenna element, as depicted in Figure 3.2(a), and thus, making number of transmit elements, $N_{TX} = 64$. There are no sub-arrays and thus, the precoder for beamforming is optimized for all 64 antenna elements. The antenna gain of an antenna element is configured according to the 3GPP model as indicated in Table 7.3-1 of [18], with a maximum antenna gain per element of 8 dBi. The horizontal and vertical cut of the antenna radiation pattern of a single antenna element is also shown in Figure 3.3. We

assume that all users and the RIS are in the far-field of a cell (i.e. all antenna elements of the cell have the same gain to all the elements of the RIS and to all the antenna elements of a given user). The spacing between adjacent antenna elements is equal to $\lambda/2$. The antenna element gain of a cell $c$ towards a user $u$ is denoted as $A_{D,cu}$, and towards the RIS is denoted as $A_{I,c}$. (The use of $D$ and $I$ in the subscript denotes the two different types of links, a direct link between cell and user and an indirect path from cell to RIS, respectively as they are explained in better detail in Section 3.4).

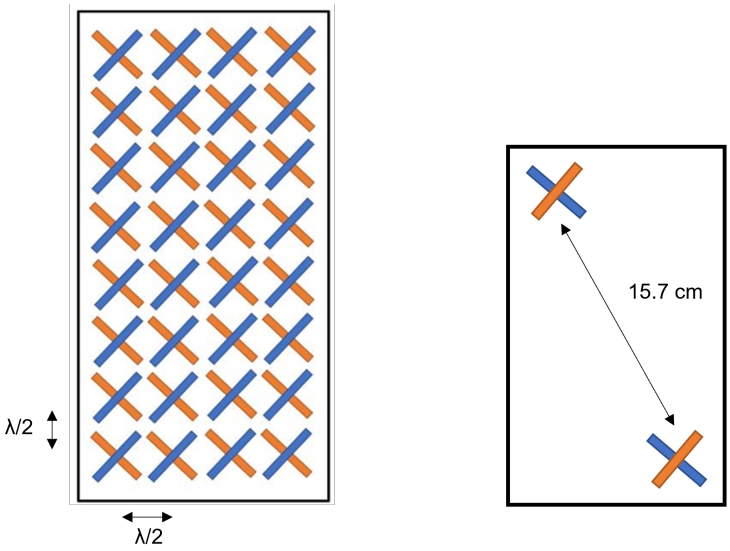


a) BS antenna panel b) UE antenna

Figure 3.2: a) Antenna array deployed at a site with half-wavelength horizontal and vertical spacing between adjacent antenna elements b) Antenna placement at a user terminal

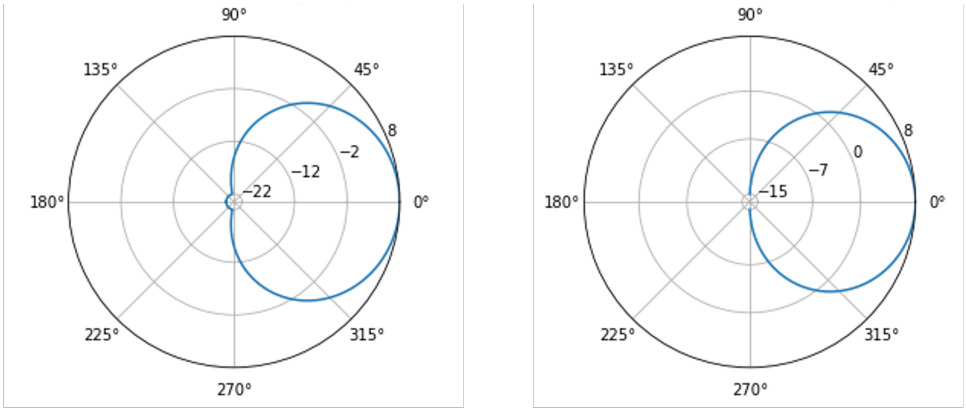


a) Horizontal cut of the antenna gain pattern (dB) b) Vertical cut of the antenna gain pattern (dB)

Figure 3.3: Horizontal and vertical cuts at elevation = 0°and azimuth = 0°respectively, are shown for a single antenna element of a BS

Each UE (user equipment) is assumed to have two pairs of cross-polarised antenna elements, placed in opposite corners of their terminal, as shown in Figure 3.2(b). Thus, the number of receiver antennas as denoted by $N_{RX}$, is equal to four. The antenna gain of all UE antenna elements is assumed to be 0 dBi.

Given the UE antenna height, the BS antenna height, and the ISD, the mechanical downward tilt is derived for the cells to be 5°. An appropriately configured downward tilt ensures the coverage of cell edge users in case of no shadowing and multipath fading, and reduces interference for users of outer cells.

### Antenna pattern for the outermost 12 cells

As mentioned above, to simplify the interference model and to reduce the simulation time in a multi-cell layout scenario we do not model any explicit users (and hence, no user-oriented beamforming) in the outermost twelve cells. Instead we assume those cells are transmitting at a fixed maximum transmit power $P_T$, and assume an antenna diagram as depicted in [19]. We use the same with a downward mechanical tilt of 5°as other cells. Horizontal and vertical gains of this model are described in Figure 3.4, which are summed together to get the total antenna gain in a given direction.

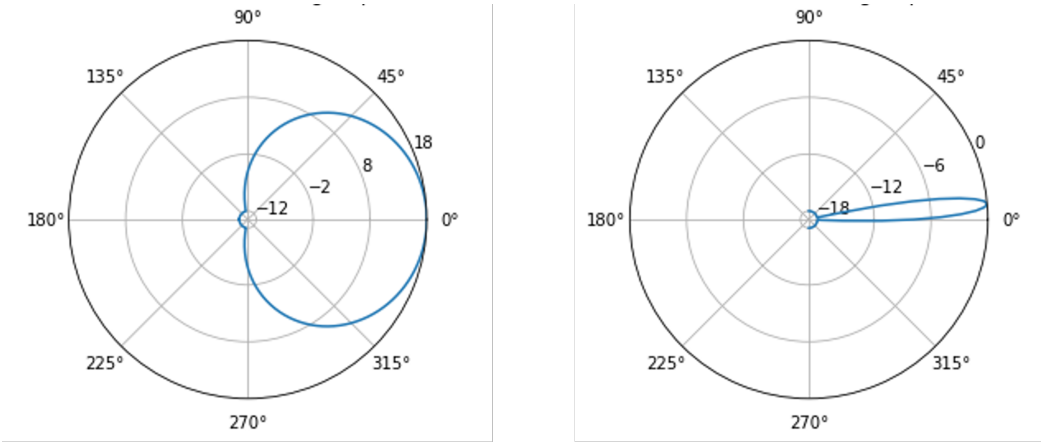


a) Horizontal antenna gain (dB)

a) Vertical antenna gain (dB)

Figure 3.4: Horizontal and vertical antenna gains for an outer cell.

## 3.3 RIS modeling

This section describes the modeling of the RIS as used in this thesis.

The RIS is an array of $M$ meta-surface elements with sub-wavelength size and spacing. The size of each element is defined as $\lambda/2 \times \lambda/2$, where $\lambda$ denotes the carrier wavelength and the spacing between adjacent elements is also $\lambda/2$. The surface of the RIS is depicted in Figure 3.5.

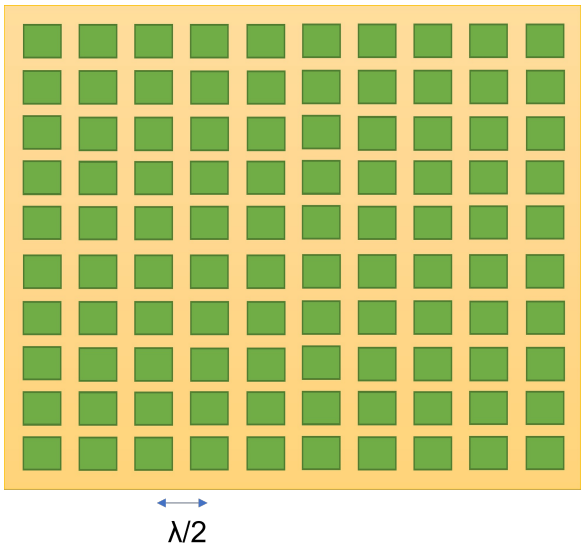


Figure 3.5: RIS Surface with $M$ RIS elements where each green square represents an element

We assume the dimensions of the surface on which the RIS is deployed to be fixed of size $40 \times 40$ RIS elements. Each RIS element reflects the signal with a controllable phase shift and no amplitude attenuation. These phase shifts are represented through a RIS configuration matrix $\mathbf{\Phi}$ which is a diagonal matrix with elements of the vector $\{e^{j\theta_0}, e^{j\theta_1}, ..., e^{j\theta_{M-1}}\}$, where $\theta_n$ represents the phase shift of the $n^{th}$ RIS element. One of the ways to control the phase shifts of the RIS is using diodes, which allow each element to reflect only with a fixed phase resolution. However, for simplicity, we deal with continuous variables for phase shifts in our simulations. While this may not accurately reflect real-world scenarios, research has shown that discretizing phases to quantize into three or more bits does not result in a significant performance loss [20].

As a default setting, when the RIS is not optimized, we choose $\mathbf{\Phi} = \boldsymbol{I_M}$, an identity matrix of size $M$. We consider this as a default RIS configuration noting that when all elements are configured to a common phase shift, the RIS acts as a mirror, meaning that the RIS reflects with maximum power in the direction where the incident angle is equal to the reflected angle [21]. This default RIS configuration is denoted as $\mathbf{\Phi}_d$.

## 3.4 Channel modeling

Now given $N_{TX}$ antennas at each BS, $M$ RIS elements, and $N_{RX}$ antennas at each UE, a channel exists at a TTI $t$ and at PRB $f$, represented by the channel response matrix $\mathbf{H}(t, f)$, between each of the following three links (see Figure 3.6):

1. direct link D between cell $c$ and user $u$:
   $\mathbf{H}_{D,cu}(t, f) \in \mathbb{C}^{N_{TX} \times N_{RX}} \; \forall \; u \in \mathcal{U} \; , \; c \in \mathcal{C} \; , \; f \in \mathcal{F}$

2. link between cell $c$ and the RIS, denoted by I (incident signal on RIS):

$\mathbf{H}_{I,c}(t,f) \in \mathbb{C}^{N_{TX} \times M} \; \forall \; c \in \mathcal{C} \; , \; f \in \mathcal{F}$

3. link between the RIS and user $u$, denoted by R (reflected signal from RIS):
   $\mathbf{H}_{R,u}(t,f) \in \mathbb{C}^{M \times N_{RX}} \; \forall \; u \in \mathcal{U} \; , \; f \in \mathcal{F}$

The link between a cell and a user via the RIS is mentioned henceforth as the indirect link (or path). We now use a cascaded channel model to describe the complete channel where the indirect link is affected by phase-controlled RIS elements [11]. The complete channel between a cell $c$ to user $u$ via the RIS is described in the following equation:

$$\mathbf{H}_{c,u}(t,f) = \mathbf{H}_{D,cu}(t,f) + \mathbf{H}_{I,c}(t,f)\mathbf{\Phi}(t)\mathbf{H}_{R,u}(t,f) \; \forall \; c \in \mathcal{C}, \; u \in \mathcal{U} \tag{3.1}$$

where, $\mathbf{\Phi}$ is the phase configuration matrix of RIS $r$ at time $t$ as described in Section 2.2.

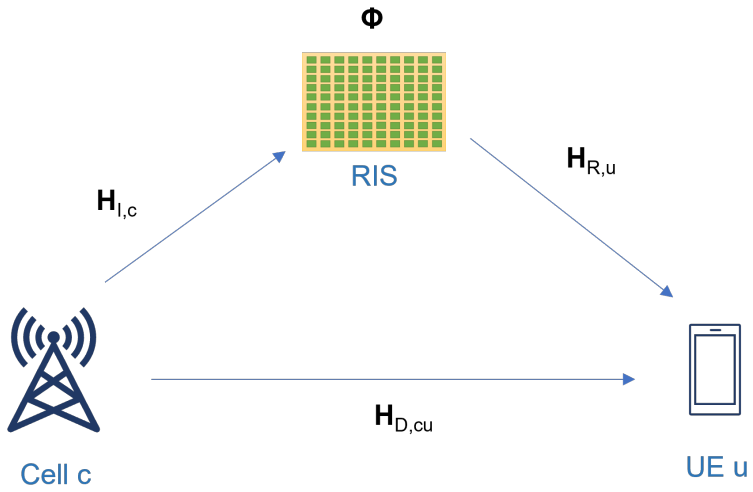


Figure 3.6: The channel is described for each link, including the cell-UE, cell-RIS, and RIS-UE links. The RIS configuration matrix for the RIS is denoted as $\mathbf{\Phi}$.

In our model, we chose to do wideband precoding and combining which means that the precoding and combining is done over a wideband-equivalent channel. This wide-band channel is represented as $\bar{\mathbf{H}}_{c,r,u}(t)$ and can be calculated by:

$$\bar{\mathbf{H}}_{c,u}(t) = \frac{\sum_{f \in \mathcal{F}} \mathbf{H}_{c,u}(t,f)}{(|\sum_{f \in \mathcal{F}} \mathbf{H}_{c,u}(t,f)|)} * \frac{\sum_{f \in \mathcal{F}} |\mathbf{H}_{c,u}(t,f)|}{F} \tag{3.2}$$

In Equation 3.2, average of the absolute channel gains over all PRBs is multiplied with the normalized sum of the channel over all PRBs.

Each channel comprises of an average channel gain $H^{av} \in \mathbb{R}$ and a time and frequency-varying multi-path fading channel $\mathbf{H}^{small-scale}(t,f) \in \mathbb{C}$. This is described for a general link $l$ between $x$ and $y$ entities by:

$$\mathbf{H}_{l,xy}(t,f) = \sqrt{H^{av}_{l,xy}} * \mathbf{H}^{small-scale}_{l,xy}(t,f) \tag{3.3}$$

Section 3.4.1 provides a detailed description of the average channel gain, while Section 3.4.2 focuses on the multi-path fading channel.

### 3.4.1 Average channel gain

We model the average channel gain for the three given links (i.e. cell to user, cell to RIS, and RIS to user) considering various factors such as path loss ($PL$), shadowing ($S$), antenna gains ($A$), building penetration loss ($BPL$) for indoor users, RIS orientation loss ($ROL$), human body loss ($HBL$), and blocking loss ($X$). A minimum coupling loss ($L_{coupling}$) of 70 dB is assumed to avoid unrealistically small losses over short distances. The channel gain for the three links can be described as follows:

1. direct link between cell $c$ and user $u$:
   $H^{av}_{D,cu}(dB) = A_{D,cu} - max(PL_{D,cu} + S_{D,cu}, L_{coupling}) - BPL_u - HBL - X_{D,cu}$
   $\forall\ u \in \mathcal{U}\ ,\ c \in \mathcal{C}$

2. between cell $c$ and the RIS:
   $H^{av}_{I,c}(dB) = A_{I,c} - max(PL_{I,c} + S_{I,c}, L_{coupling}) - ROL_{I,c}$
   $\forall\ c \in \mathcal{C}$

3. between the RIS and user $u$:
   $H^{av}_{R,u}(dB) = -max(PL_{R,u} + S_{R,u}, , L_{coupling}) - BPL_u - HBL - X_{R,u} - ROL_{R,u}$
   $\forall\ u \in \mathcal{U}$

Each of these losses is described in detail below.

#### Path loss

A log-distance path loss model is used to describe the distance-based path loss between all links, given by the equation:

$$PL = PL_0 + 10\gamma \log_{10}(d/d_0) \tag{3.4}$$

where $PL$ and $PL_0$ are in dB, and $PL_0$ is calculated using the Friis free space path loss model at a reference distance of $d_0 = 1$m [22].

#### Shadowing

The shadow fading, or slow fading, is represented by a zero-mean Gaussian random variable $S$ with standard deviation $\sigma_{sh}$. $\sigma_{sh}$ is taken to be 7 dB for all links in an indoor users scenario and 6 dB in outdoor users scenario [18].

To model the spatial and inter-site correlation, shadowing maps are derived for each cell using the method provided in [23] considering a pixel size of 5m. These maps are derived to model spatial correlation, defined by a decorrelation distance of 50m, and an inter-site correlation of 0.5 [23]. Thus, shadowing for a user $u$ from cell $c$ can be derived using the shadowing map for cell $c$ at the location of user $u$. Shadowing experienced on a cell-RIS link is found using the shadowing map of cell $c$ at the location of RIS $r$. Similar to those of cells, shadowing maps are created for all the RISs where shadowing can be found for the position of each user $u$ from RIS $r$ using the shadowing map of RIS $r$ at the location of user $u$. An example of a shadowing map is depicted in the Figure 3.7.

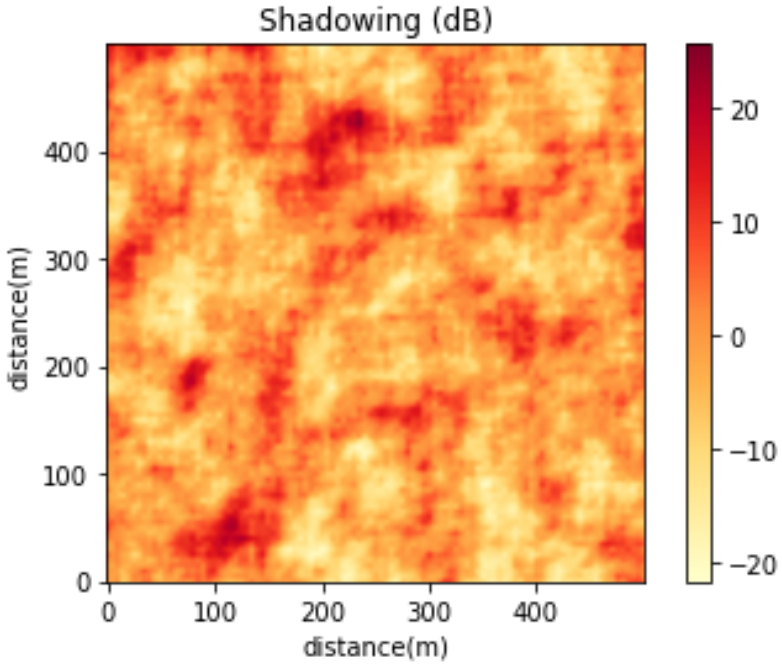


Figure 3.7: One of the generated shadowing maps is shown for an area of 500m × 500m for outdoor users.

### Blocking loss

In this thesis, we have considered a dense urban environment which is unpredictable by nature. For example, temporary blocking conditions may be created, such as those caused by large trucks. This temporary blocking effect is represented by a random variable $X$. The blocker can be present between the cell and the user and/or between the RIS and the user with a certain blocker probability, denoted as, $P_{BL}$. When blocker is not present, then $X$ takes the value to be 0 dB, otherwise it selects the pre-configured value $BL$.

Since both the cell antennas and the RIS are deployed at a height of more than 15m, and we assume the RIS to be strategically deployed, we make a fair assumption that such a blocker will never be present between them.

For a given scenario, values of $BL$ and $P_{BL}$ are fixed. We simulate different scenarios by varying the blocker loss or blocker probability to understand their impact on the performance of a RIS-aided network.

### Other losses

Human body loss refers to the attenuation caused by the presence of a human body between the cell and UE terminal, and we assume a constant loss of HBL = 6 dB [24].

Building penetration loss ($BPL_u$) for the scenario with indoor users is calculated using the building penetration model described in Table 7.4.3-3 of [18]. For the scenario with outdoor

users, we consider it to be 0 dB.

Since the RIS is deployed at a building, there won't be any indirect path when a cell or user is behind the building. In such scenarios, we model a RIS orientation loss (ROL) of infinite dB, which is otherwise 0 dB.

### 3.4.2 Time-and-frequency-varying channel modeling

After discussing the average channel gains, we now address the scale-scale fading in this section.

Let's first consider the cell-RIS channel. We assume this channel to always be LoS (line of sight) since both are deployed at a height of 25m and 20m, respectively. Given the line of sight nature and the fixed locations of the cell and the RIS, we assume that there is no multipath fading on the cell-RIS link. We model the small-scale fading between the cell $c$ and RIS $r$ using the following equation:

$$\mathbf{H}_{I,cr}^{small-scale}[i,j] = e^{j2\pi d_{ij}/\lambda} \; \forall \; i \in \{0,1,..,N_{TX}-1\}, j \in \{0,1,..,M-1\} \tag{3.5}$$

where $d_{ij}$ is the distance between the $i^{th}$ antenna element of cell $c$ and the $j^{th}$ RIS element, and $\lambda$ is the carrier wavelength.

Between the cell and the user, as well as between the RIS and the user, there lies a more complicated time-varying model due to users moving locally at a pedestrian speed. We use QuaDRiGa to implement the 3GPP modeled channel for this [25]. We model the local character of the user mobility by creating a circular track of radius 0.5m where the user moves at a speed of 0.8m/s. We specify the scenario for the model as the UMa LoS model, as described in [18].

Ideally, we would use this model for each sampled user, but that would lead to a complex slot-level implementation. So we create a randomized set of generic traces at arbitrary user positions and then for each specific cell-RIS and RIS-user link, we randomly select one of the generic traces and convert the trace to the specifics of the involved cell/UE orientations. In order to do this, first, we remove the phases from the channel traces generated for the arbitrary user positions, thus making them phaseless using the following equation:

$$\mathbf{H}_{trace,phaseless}^{small-scale}[i,j] = e^{j2\pi d_{ij}/\lambda} * \mathbf{H}_{trace,original}^{small-scale}[i,j] \\ \forall \; i = 0,1,..,N_{TX}-1, j = 0,1,..,N_{RX}-1 \tag{3.6}$$

where $d_{ij}$ is the distance between $i^{th}$ antenna element of the cell, and $j^{th}$ antenna element of user with the trace-specific arbitrarily-defined user location.

Next, for each cell-user and RIS-user link, we randomly select one of these processed generic traces, along with a random starting point. Finally, a distance-based phase (distance for the actual user location) is added back to the trace using:

$$\mathbf{H}_{c,u}^{small-scale}[i,j](t,f) = e^{-j2\pi d_{ij}/\lambda} * \mathbf{H}_{trace,phaseless}^{small-scale}[i,j] \\ \forall \; i = 0,1,..,N_{TX}-1, j = 0,1,..,N_{RX}-1 \tag{3.7}$$

To further save on the memory use of these traces, we store channel responses only for every fourth TTI, using interpolation within the simulator to calculate the small-scale fading channel to calculate for the rest of the TTIs.

Now that we have modeled the network and the channel, we move forward in formulating the problem, scoping it, and establishing different algorithms to solve it.

# Chapter 4

# Problem statement and heuristic solution

We defined the research problem addressed in this thesis in Chapter 1 as the ***optimization of radio resource management in a RIS-aided 6G network to improve the throughput performance***.

As a part of this, we have the following resource management tasks in the proposed setup, as also visualized in Figure 4.1:

1. Cell-UE association: The set of users associated with a given cell $c$ is denoted by $\mathcal{U}_c \subset \mathcal{U}$. For example, in Figure 4.1, all blue users are associated with the cell on the right.

2. User scheduling: The set of users for cell $c$ that are scheduled in TTI $t$ is denoted by $\mathcal{U}_c^S(t) \subset \mathcal{U}_c$. The set of all scheduled users of all cells is denoted by $\mathcal{U}^S(t) = \bigcup_{c \in \mathcal{C}} \mathcal{U}_c^S(t)$. We use the proportional fairness-based scheduler to schedule users to achieve fairness in user throughput. In Figure 4.1, two of the blue users are scheduled in the given TTI.

3. Cell-RIS association: By cell-RIS association, we mean that the associated cell can utilize and configure the RIS for the benefit of its users. The set of cells associated with the RIS in the TTI $t$ is denoted by $\mathcal{C}^{RIS}(t) \in \mathcal{C}$. In Figure 4.1, we see that for the RIS, two cells are associated at this time. When a RIS is unable to improve performance for any user scheduled, then this will be an empty set.

4. RIS-UE association: By RIS-UE association, we mean that the RIS configuration in the given TTI is optimized to best support the users it is associated with. In Figure 4.1, we observe the RIS to be configured to support three users. The set of users associated to the RIS in TTI $t$ is denoted by

$$\mathcal{U}^{RIS}(t) \subset \bigcup_{c \in \mathcal{C}^{RIS}(t)} \mathcal{U}_c^S(t)$$

.

5. Beamforming:

   (a) The transmit precoding matrix for cell $c$ at TTI $t$ is denoted by $\mathbf{W}_c(t)$, where $\mathbf{W}_c(t)$ is composed of precoding vectors $\mathbf{w}_{c,u}(t) \in \mathbb{C}^{N_{TX}}$ for all users $u \in \mathcal{U}_c^S(t)$ and $c \in \mathcal{C}$, recalling that $N_{TX}$ is the number of antenna elements of a transmit antenna at the BS. The precoder is optimized for all the scheduled users at time $t$, as depicted by the beams in Figure 4.1.

   (b) The phase configuration matrix of the RIS at time $t$ is a diagonal matrix denoted by $\mathbf{\Phi} \in \mathbb{C}^{M \times M}$. The RIS is configured to reflect the beam in the optimal direction towards the scheduled users it is associated with, as shown in Figure 4.1.

   (c) The receiver combiner at user $u$ at time $t$, that combines the signals received at all UE antenna elements, is denoted by $\mathbf{v}_u(t) \in \mathbb{C}^{N_{RX}}$ for all scheduled users $u \in \mathcal{U}^S(t)$, where $N_{RX}$ is the number of receive antenna elements at the UE.

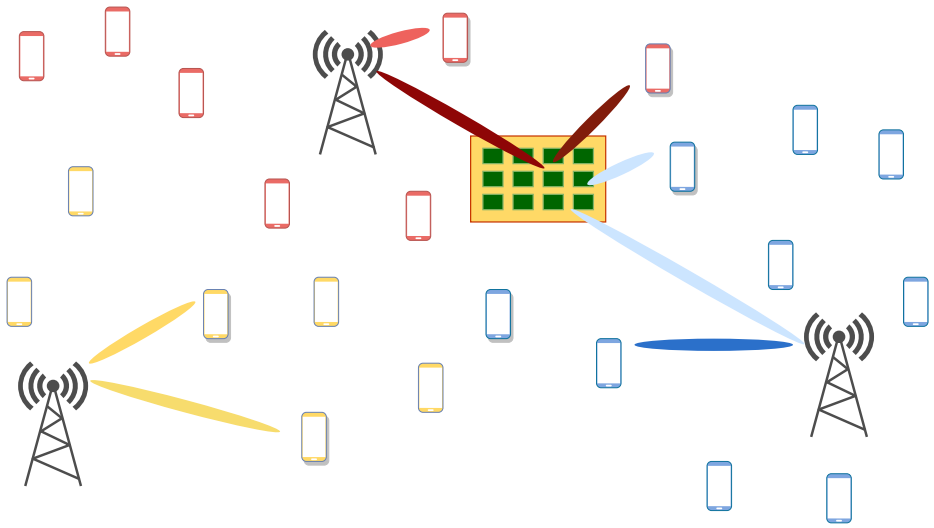

Figure 4.1: Setup illustrating the radio resource management decisions at a given time $t$ when multiple base stations and multiple RISs are deployed.

## 4.1 Scoping the problem

Given the complexity of the problem, and to solve it using heuristic algorithms, we make the following assumptions:

1. Users' association with a cell is fixed for the duration of the call. Users select the cell towards which they receive the maximum average channel gain. This decision is represented by the following formula:

$$c^u = \arg\max_{c \in \mathcal{C}} |H_{D,cu}^{av} + H_{I,c}^{av} * H_{R,u}^{av}|^2 \; \forall \; u \in \mathcal{U} \tag{4.1}$$

   where, $c^u$ denotes the cell with which a user $u$ is associated with.

Note that a user is not associated with any cell if the maximum of the average channel gains it receives from all cells is 0, i.e., no channel exists from all cells. This also implies that we do not have a coverage check based on RSRP (reference signal received power) exceeding some threshold and that the user has no coverage if and only if its (direct or indirect) paths to all cells are blocked.

2. RIS has fixed association to the innermost cell 0 (our cell of interest). This is a fair assumption since considering the RIS deployment, the path loss in the indirect link is too high for any other cells to gain from associating with the RIS. Thus, $\mathcal{C}^{RIS}(t) = \{0\}\ \forall\ t$ and $\mathcal{U}^{RIS}(t)\ \subset \mathcal{U}_0^S(t)$.

3. At a given TTI $t$, the RIS can only be associated with one user of the network. Thus, $|\mathcal{U}^{RIS}(t)| \in \{0, 1\}$.

4. At a given TTI $t$ and PRB $f$, the combiner at all users $u$, associated with cell $c^u$, is optimized independently using the MRC combiner described in Section 2.4 and given by equation:

$$\mathbf{v}_u(t, f) = (\sqrt{P_T^u}\mathbf{w}_{c^u,u}(t)\mathbf{H}_{c^u,u}(t, f))^+\ \forall\ u \in \mathcal{U} \tag{4.2}$$

where $P_T^u$ is the transmit power per PRB provided for user $u$

These assumptions limit our problem to solving only for beamforming (active and passive), user scheduling, and RIS-UE association. This problem is illustrated in Figure 4.2, where we see that each user gets associated with a cell, then a subset of the users are scheduled at the given TTI, RIS is associated to a fixed cell (red cell) and is optimized for one of the scheduled users of that cell, and finally, BS precoding is optimized for each scheduled user.

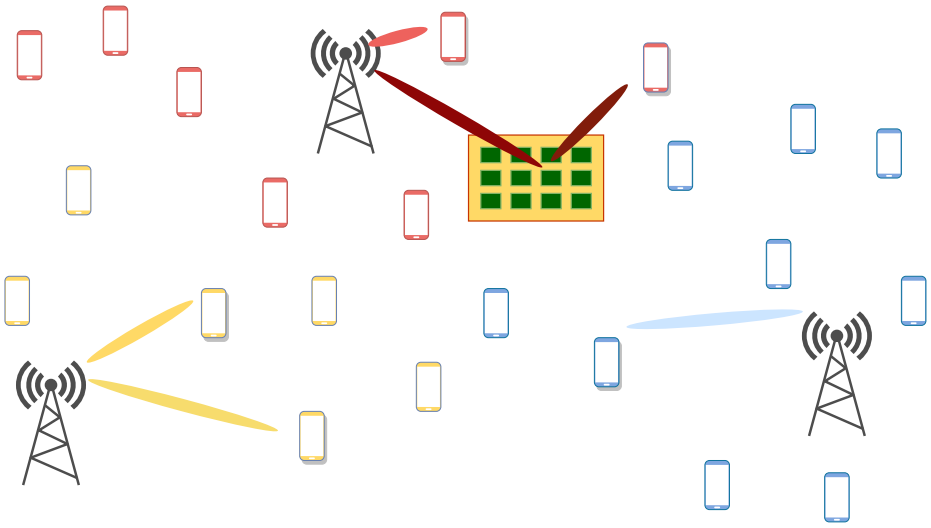

Figure 4.2: This figure represents the limited scope of the problem that will be discussed in the remainder of the thesis.

Before diving deeply into the solution, let us look at the interference and noise modeling that helps us evaluate SINR and throughputs.

## 4.2 SINR and throughputs calculation

As the backbone of our algorithms relies on throughput estimation, which is intricately linked to the calculation of SINRs, we explain the modeling interference and noise, as well as the methods employed for SINR computation and throughput assessment.

It is important to note that communication occurs solely on a single layer for all users. In other words, at any given moment, a user receives data on just one channel, without exploiting the advantages of SU-MIMO-based spatial multiplexing. Additionally, we assume that perfect Channel State Information (CSI) is available to the cells for their respective users. Uplink Sounding Reference Signal (SRS) signals transmitted by users can be harnessed to obtain CSI for the direct channel. Meanwhile, a pilot-based channel retrieval scheme can be employed for indirect links.

### 4.2.1 SINR calculation

We calculate the $SINR_{u_0}(t, f)$ for the user $u_0$, associated to cell $c_0 = c^{u_0}$, at the TTI $t$ and PRB $f$ as:

$$SINR_{u_0}(t, f) = \frac{1}{(\sum |\mathbf{v}_{u_0}(t, f)|^2)N_0 + I_{u_0,intra}(t, f) + I_{u_0,inter}(t, f)} \tag{4.3}$$

where, $\mathbf{v}_{u_0}(t, f)$ is the combiner of this user $u_0$. $N_0$ is the noise power and $I_{u+0,intra}(t, f)$, $I_{u+0,inter}(t, f)$ denotes the intra-cell and inter-cell interference, respectively. These are described in detail in the next part.

#### Noise modeling

Noise Power $N_0$ is calculated using the formula:

$$N_0 = KTB \times 10^{NF/10} \tag{4.4}$$

where $K$ is the Boltzmann constant, i.e., $1.38 \times 10^{-23}$ Joules-per-Kelvin, $T$ is the thermal noise temperature taken as 290 Kelvin, $NF$ is the receiver noise figure of 8 dB, and $B$ is the bandwidth over which we calculate the SINRs, which in our case is the bandwidth of a PRB.

#### Interference modeling

1. Intra-cell interference: This term refers to the interference received by a user $u_0$ from the users of its own cell $c_0$ using the same resource block of TTI $t$ and PRB $f$. This interference can be calculated as:

$$I_{u_0,intra}(t, f) = \sum_{u_j \in \mathcal{U}_{c_0}^S(t) \setminus \{u_0\}} P_T^{u_j}(t) |\mathbf{v}_{u_0}(t, f) \mathbf{H}_{c_0,u_0}(t, f) \mathbf{w}_{c_0,u_j}(t)|^2 \tag{4.5}$$

   where, $P_T^{u_j}(t) = P_{T,PRB}^{c_0}(t)$ is the transmit power per PRB to user $j$, which is equal to the total transmit power of cell, divided by the number of PRBs, divided by the number of scheduled users.

2. Inter-cell Interference: This term refers to the interference encountered by a user $u_0$ from users in neighboring cells utilizing the same resource block in TTI $t$ and PRB $f$. In a single-cell layout, detailed in Section 3.1, this value is effectively zero. In contrast, within a multi-cell arrangement, we differentiate between the inner seven cells and the outer twelve cells, as outlined in Sections 3.1 and 3.2. The computation of inter-cell interference involves the following components:

$$I_{u_0,\text{inter}}(t,f) = I_{u_0,\text{inter,inner}}(t,f) + I_{u_0,\text{inter,outer}}(t,f) \tag{4.6}$$

where,

$$I_{u_0,\text{inter,inner}}(t,f) = \sum_{c_i \in \{0..6\} \setminus \{c_0\}} \sum_{u_j \in \mathcal{U}_{c_i}^S(t)} P_{T,PRB}^{c_i} |\mathbf{v}_{u_0}(t) \mathbf{H}_{c_i,u_0}(t,f) \mathbf{w}_{c_i,u_j}(t)|^2 \tag{4.7}$$

and,

$$I_{u_0,\text{inter,outer}}(t,f) = \sum_{c_i \in \{7..18\}} P_{T,PRB} |\mathbf{v}_{u_0}(t) \mathbf{H}_{c_i,u_0}(t,f) \mathbf{w}_{\text{uniform}}|^2 \tag{4.8}$$

It should be noted that the outer twelve cells are assumed to transmit at maximum power with antenna gain, as detailed in Section 3.2. Since no users are accounted for in these cells, we utilize a uniformly normalized precoding matrix denoted as $\mathbf{w}_{\text{uniform}}$, which simply divides the transmit power equally to all the antenna elements.

We model CQI (channel quality indicator) reporting such that the user-experienced inter-cell interference is available at the serving cell, which it can then use to estimate the SINR and thus estimate the data rate. We measure the inter-cell interference, averaged over all PRBs, during the last DL slot preceding the UL slot in which we feed back the CQI. Subsequently, the cell employs this information to estimate the SINR for users over the subsequent four downlink slots. To illustrate, if the downlink starts at TTI 0, the subsequent uplink takes place at TTI 4. Consequently, the inter-cell interference is measured at TTI 3 and is utilized for user $u$ from TTI 5 to 8. This is shown in the equation below:

$$\hat{I}_{u,inter}(5) = ... = \hat{I}_{u,inter}(8) = \sum_{f \in \mathcal{F}} I_{u,inter}(3,f)/N_{PRB} \tag{4.9}$$

In the previous step, we computed the SINR per PRB basis. However, our focus is on evaluating SINR over the whole carrier. The method employed for this purpose is known as Mutual Information Effective SINR Mapping (MIESM). This approach aids in computing the effective SINR ($SINR_u^{eff}$) for a given user $u$ spanning all PRBs. The calculation of effective SINR involves two key stages: the transformation of each $SINR_u(t,f)$ value into mutual information, $MI_u(t,f)$, followed by the derivation of the average $MI_u(t,f)$, denoted as $MI_u^{eff}(t)$, which is then mapped back to yield $SINR_u^{eff}(t)$. This mapping is based on the MCS-dependent curves, illustrated in Figure 4.3 [2]. We choose the curve corresponding to 256 QAM modulation for this thesis. Since we use a Shannon-based data rate calculation, and not adopt a MCS (modulation and coding scheme) dependent rate control algorithm, we assume the MCS to be 256 QAM, which provides the best data rate and spectral efficiency.

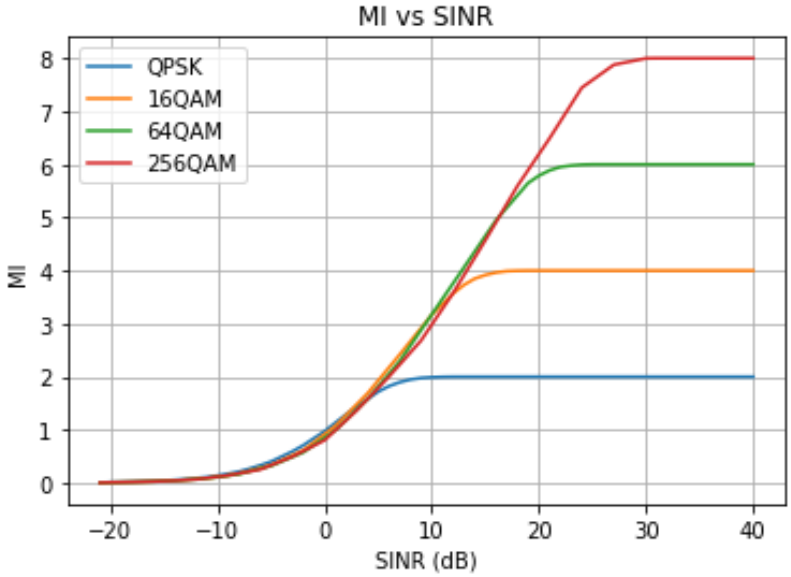


Figure 4.3: MI vs SINR curves for different modulation orders. [2]

### 4.2.2 Throughput calculation

Next, we can obtain the data rate for user $u$ using the truncated Shannon rate, as shown below:

$$R_u = \min\{R_{max}, CF * Blog_2(1 + SNR_u^{eff})\} \tag{4.10}$$

Here, $R_{max}$ is the maximum achievable rate of 114.752 Mbps, as calculated using the steps given in Section 5.1.3.2 of [26]. The correction factor $CF$ is used to model the resources taken away by control signaling and the inaccuracies in channel estimations. The numerical value of 0.75 for $CF$ is selected based on the range of such correction factors documented in [27].

Having addressed the calculations of SINR and throughput, we will now return to the discussion of defining solutions for the proposed problem and present the different algorithms that will address the problem of beamforming, user scheduling, and RIS-UE association in the subsequent section.

## 4.3 Algorithms to optimize radio resource management tasks

Below, we present the three algorithms to solve the problem of optimization of radio resource management tasks, such as beamforming, user scheduling, and RIS-UE association:

1. Benchmark: This approach serves as a baseline for comparison, and thus, the RIS is deployed but remains unused (retaining the default phase shift matrix). Hence, we **jointly optimize only scheduling and precoder** for BS beamforming.
2. Algorithm 1: This algorithm builds on the benchmark by **first only optimizing scheduling** without considering RIS but **then tries to configure the RIS** to op-

timize the user throughput for any scheduled user and then finally **optimizes the precoder**.

3. Algorithm 2: In this algorithm, we investigate RIS-aware scheduling. Algorithm 2 involves **simultaneously optimizing scheduling, precoding, and RIS configuration** to achieve the best throughput fairly.

While we explored many scenarios in our simulation experiments, the sections below give an overview of each of the algorithms as applied in a multi-cell MU-MIMO scenario that will encompass all other scenarios.

### 4.3.1 Benchmark algorithm

In this benchmark algorithm, we fix the configuration of RIS, $\mathbf{\Phi}$ to the default matrix $\mathbf{\Phi}_d = \boldsymbol{I_N}$. Then, at each TTI $t$, preliminary precoder $\tilde{\mathbf{w}}_{u,rx}(t)$ is calculated for each receiver antenna $rx$ of user $u_0$ using MRT precoder as given by Equation 4.11.

$$\tilde{\mathbf{w}}_{u_0,rx}(t) = \frac{\bar{\mathbf{H}}_{c^{u_0},u_0}(t)[:,rx]^*}{||\bar{\mathbf{H}}_{c^{u_0},u_0}(t)[:,rx]||_2} \tag{4.11}$$

Rates, $\hat{R}^{default}_{u,rx}(t)$, are then estimated for each user-$rx$ pair using the method described in Section 4.2.1 based on the MRT-based precoder, $\tilde{w}_{u,rx}(t)$ and the CQI received.

Given the estimated data rates for all users and each rx antenna choice, we now follow the algorithm as shown in Figure 4.4.

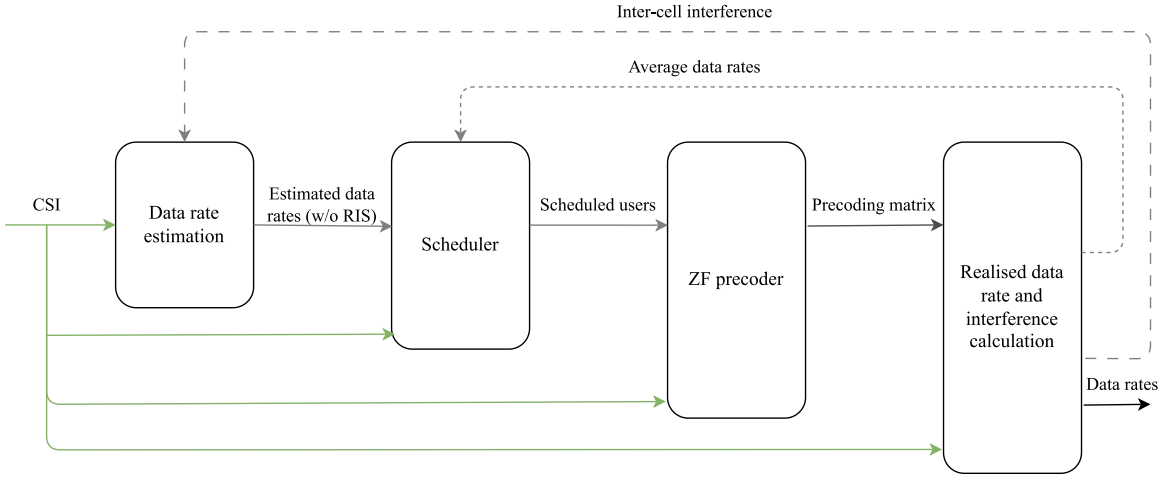


Figure 4.4: Benchmark:algorithm followed at a given time $t$ to optimize precoding and scheduling. True CSI of a given TTI is the input for all blocks. The average data rate from the previous TTI is taken as input to the scheduler, and inter-cell-interference from the last uplink slot is taken as input for data rate estimation.

We employ proportional-fair scheduling by calculating first a priority matrix based on the

proportional fairness index, $PF_{u,rx}$ for every user-receiver pair as given in Equation 4.12).

$$PF_{u,rx} = \frac{\hat{R}_{u,rx}^{default}(t)}{R_u^{av}(t-1)} \tag{4.12}$$

Next, multi-user scheduling is conducted using the semi-orthogonal user selection (SUS) algorithm as described in [16]. With this algorithm, users are scheduled in order of decreasing priority as long as the channel of each new co-scheduled user is sufficiently orthogonal with the channel of the already scheduled users of a given cell. To do this, we introduce $\mathbf{g_k}$ as the span of the channel when $k$ users are scheduled and $\gamma$ as the orthogonality index. SUS algorithm is conducted in the following steps for a cell $c$ at time $t$:

1. Step 1 (initiation):
$$u_0, rx_0 = \arg\max_{u \in \mathcal{U}_c} PF_{u,rx} \tag{4.13}$$
User $u_0$ with best PF index is scheduled and $\mathbf{g_1} = \mathbf{H}_{c,u_0}[:, rx_0]$.

2. Step 2 (considering $k$ users are co-scheduled by far):
For the use $u_i$ and $rx_i$, which has the next best PF, we calculate:
$$\gamma = \frac{|\mathbf{g_{(k-1)}}^* \mathbf{H}_{c,u_i}[:, rx_i]|}{||\mathbf{g_{(k-1)}}||_2 ||\mathbf{H}_{c,u_i[:,rx_i]}||_2} \tag{4.14}$$
If $\gamma > \gamma_{th}$, then the user $u_i$ is co-scheduled and we update $\mathbf{g_k}$ as:
$$\mathbf{g_k} = \mathbf{H}_{c,u_i}[:, rx_i](\mathbf{I} - \sum_{j=1}^{k-1} \frac{\mathbf{g_j}^* \mathbf{g_j}}{||\mathbf{g_j}||_2^2}) \tag{4.15}$$

The orthogonality index, $\gamma$ is tested against a threshold value, taken as 0.5, in our case.

The output of this algorithm is the scheduled users along with their respective rx antenna index (the channel which provides the best PF index while satisfying the orthogonality check). This scheduler is visualized in Figure 4.5, which is the zoomed-out version of the 'scheduler' box in 4.4.

Finally, a precoding matrix for the users scheduled in the cell $c$ is calculated using a zero-forcing precoder as described in Equation 4.16 [17].

$$\mathbf{W}_c(t) = (\bar{\mathbf{H}}_c(t)^T)^+ = \bar{\mathbf{H}}_c(t)(\bar{\mathbf{H}}_c(t)^T \bar{\mathbf{H}}_c(t))^{-1} \tag{4.16}$$

where, $\bar{\mathbf{H}}_c(t)$ is the wideband equivalent of all the channels from the cell $c$ to the rx antenna corresponding to the rx antenna index of the scheduled users, as determined by the output of SUS algorithm.

Note that the MRT precoder was used before only to estimate per-user per-rx antenna data rates and thus to calculate PF indices. For beamforming, we actually use a ZF precoder as it has the added advantage of interference nulling which is especially important for the case of MU-MIMO.

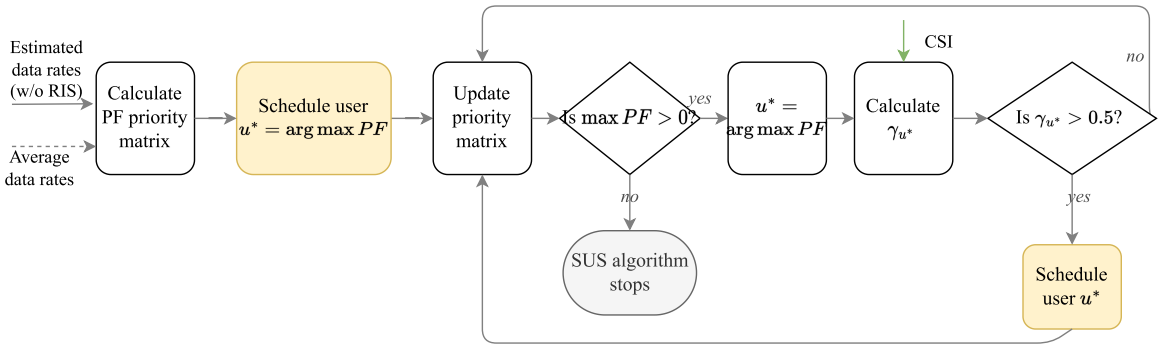


Figure 4.5: Scheduler: inputs are CSI, estimated data rates (without RIS), and average data rates up to time $t$ for all the users of the given cell. Output is the list of scheduled users for this cell at time $t$.

We then calculate the realized data rate, $R_u(t)$, for each user $u$, and the true interference using the optimized precoder. We use the realized data rate as input to update the average data rate, $R_u^{av}(t)$ following the equation below:

$$R_u^{av}(t) = \alpha R_u^{av}(t-1) + (1-\alpha)R_u(t) \tag{4.17}$$

where $\alpha$ is the exponential smoothing coefficient set to 0.1 [28].

### 4.3.2 Algorithm 1

The goal of this algorithm is to separate the scheduling and the RIS configuration decisions. Thus, it optimizes the RIS configuration matrix and the precoder once the users are scheduled. The flow of this algorithm is illustrated in Figure 4.6.

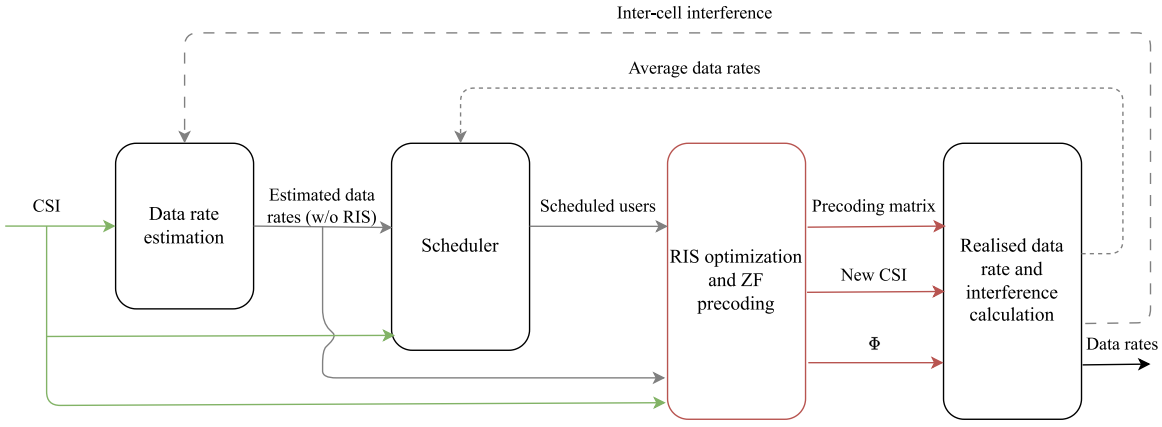


Figure 4.6: Algorithm 1: algorithm followed at a given $t$ to optimize scheduling and then jointly optimizing precoder and RIS configuration matrix $\mathbf{\Phi}$

We observe that the steps until user scheduling remain the same for this algorithm as for the benchmark algorithm. However, now instead of using the default RIS configuration, we

explore the possibility of optimizing the RIS configuration matrix for any of the scheduled users. This step of jointly optimizing the RIS configuration matrix and the precoders are visualized in Figure 4.7.

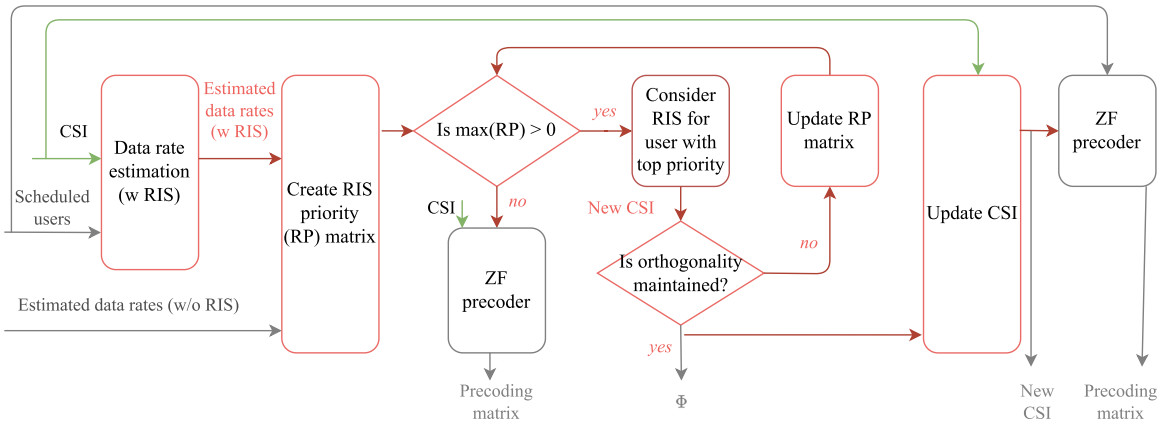


Figure 4.7: "RIS optimization and ZF precoding" block of the Algorithm 1 flowchart: CSI, scheduled users, and estimated data rates without RIS are the inputs; and Φ, new CSI, and the precoder are the outputs.

The "Data rate estimation (w RIS)" block of Figure 4.7 entails the optimization of the RIS configuration matrix considering an MRT-based precoder for each receiver antenna of each scheduled user using the method described in [11]. Equations 3.4-3.9 of [11] are used to find the optimal RIS configuration, $\hat{\mathbf{\Phi}}_{u,rx}$ which we then use to estimate the data rate with RIS, $\hat{R}^{RIS}_{u,rx}$, according to the method described in Section 4.2.1.

We next create a new RIS priority (RP) matrix for each scheduled user $u$ and receiver $rx$, using the equation below:

$$RP_{u,rx} = max(\frac{\hat{R}^{RIS}_{u,rx} - \hat{R}^{default}_{u,rx}}{\hat{R}^{default}_{u,rx}}, 0) \tag{4.18}$$

The algorithm then follows the steps in Figure 4.7 to obtain the RIS configuration matrix, updated channel, and precoder to calculate the realized data rates for all users. If $\max(RP) = 0$, that means RIS does not provide any gain to any user and is thus configured to the default configuration. ZF precoding is in the same manner as the benchmark algorithm using Equation 4.16. On the other hand, if $\max(RP) > 0$, then:

$$u_0, rx_0 = \arg\max RP_{u,rx} \tag{4.19}$$

and $\hat{\Phi}_{u_0,rx_0}$ optimized for this user-rx pair is considered. Since, configuring RIS changes the channel for all users, the orthogonality condition, as given in Equation 4.14, is checked between channels of all the co-scheduled users. Only, if this is satisfied, we configure the RIS for this user $u_0$. Otherwise, we check the condition for the next best RP. If RIS is indeed configured, then the new CSI is calculated and ZF precoding is done for all the scheduled users based on the updated channel.

### 4.3.3 Algorithm 2

In this algorithm, we aim to optimize scheduling, precoding, and the RIS configuration matrix simultaneously. This implies that the scheduling decision should take into account the potential benefits of optimizing the RIS configuration. The flow of this algorithm is similar to that of benchmark algorithm and is illustrated in Figure 4.8.

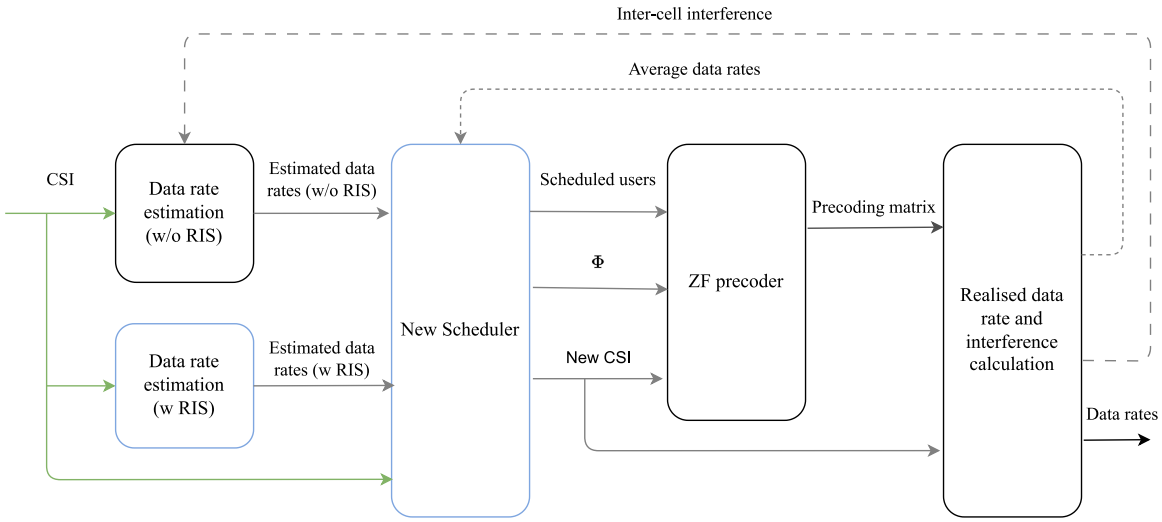


Figure 4.8: Algorithm followed at a given $t$ to optimize scheduling and then jointly optimizing precoder and RIS configuration matrix $\mathbf{\Phi}$

First, we estimate the data rate for each user when the RIS is optimized with the method described in [11]. Then, we calculate the proportional fairness index for each user $u$ and receiver pair $rx$ for both cases when RIS is in default configuration or optimized. Then the users are scheduled in order of decreasing proportional fairness index as long as all channels of co-scheduled users satisfy the orthogonality test.

There are two important things to note though for such a RIS-aware multi-user scheduling scenario. First, whenever we would like to use RIS (due to a better-estimated data rate), the channel will change, due to the configuration of RIS, for all the users in the network. So, only if all the already scheduled users and this new user can pass the orthogonality test of the SUS algorithm for this new channel, then this new user will be scheduled, with RIS configured for it. And any further user that could be scheduled at the same TTI also needs to pass the orthogonality test based on this new channel. Second, once the RIS is optimized for a user $u$, then to test whether a new user could be co-scheduled, we don't consider the estimated data rate with the RIS configured, but only the one based on the default configuration. Even though we know that due to the change in channel, this may not be the actual data rate, scheduling based on the estimated rates when RIS is in default configuration is done in order to simplify the algorithm. These changes to the original scheduler result in the design of a new scheduler as visualized in Figure 4.9.

In this chapter, we defined the problem statement, limited the scope of the problem, and provided three algorithms that can solve the problem. Next, we will compare the perfor-

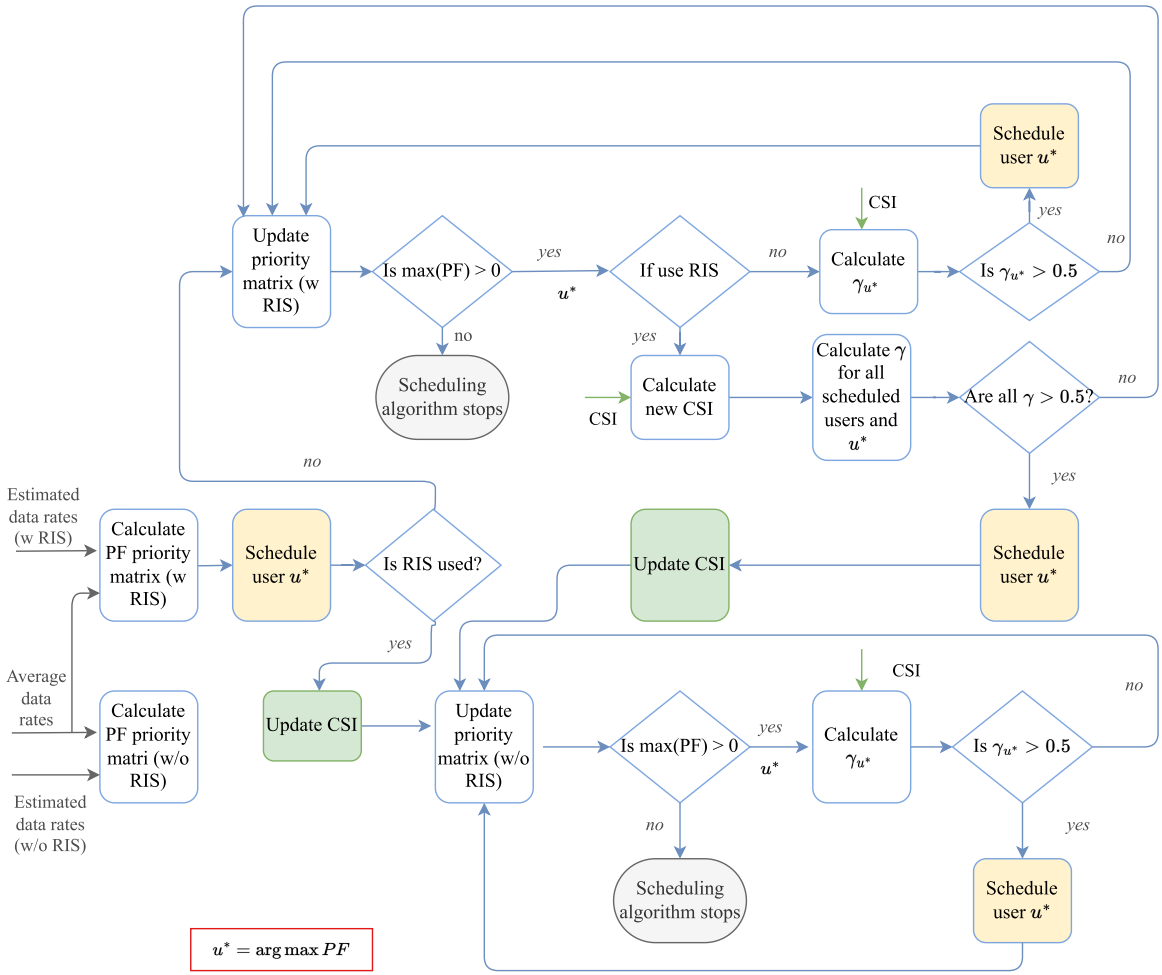


Figure 4.9: New scheduler used for Algorithm 2: Inputs are CSI, estimated data rates (with and without RIS), and average data rates up to time $t$ for all the users of a given cell $c$. Output is the list of scheduled users for this cell.

mance achieved by these algorithms in different scenarios.

# Chapter 5

# Scenarios and results

In this chapter, we analyze the performance of the proposed algorithms for different scenarios. First, we introduce the key performance indicators (KPIs) and then we present the different scenarios that are used to derive the results followed by the actual results. For each scenario, multiple snapshots, are simulated, where each snapshot represents a difference in user positions, a difference in multi-path fading (the traces used and their starting index for each user), and a difference in the presence of a blocker, independently sampled for each cell-user link and each RIS-user link. Simulations are conducted for the number of snapshots that are needed to reduce the relative halfwidth of the derived 95% confidence intervals below 5% for every KPI evaluated.

We use the following three KPIs, all defined for the innermost cell, i.e. cell 0:

- **Average cell throughput**: This denotes the cell throughput, averaged over all snapshots and all TTIs.
- $10^{th}$ **throughput percentile**: This metric denotes the $10^{th}$ percentile of the distribution of the average (over time) user throughputs of all the snapshots.
- **RIS network usage**: This metric is defined as the ratio of downlink TTIs where the optimized RIS is used to all the downlink TTIs, averaged over the snapshots.

We present results according to the four main scenarios: 1) Single-cell single-user MIMO (SCSU), 2) Multi-cell single-user MIMO (MCSU), 3) Single-cell multi-user MIMO (SCMU), and 4) Multi-cell multi-user MIMO (MCMU). Here, single-cell and multi-cell refer to the network layout used in the simulation, as described in Section 3.1, and, SU-MIMO and MU-MIMO refer to the single-user scheduling and multi-user scheduling in MIMO respectively.

As collaborated in Chapter 1, we wish to see the effect of the blocker (the strength as well as probability), the number of users, the number of RIS elements, user type (indoors or outdoors), and the deployment position of RIS on the performance evaluation of the algorithms. We define these simulation parameters in Table 5.1 with the corresponding range of values they can take. An underlined value defines the default setting for a given parameter.

| Simulation Parameters | Values |
|---|---|
| RIS deployment position | A, B, C |
| Blocker probability, $P_{BL}$ | 0.1, 0.2 |
| Blocker strength, $BL(dB)$ | 0, 15, 30, 45 |
| User type | indoors, outdoors |
| Number of users (single-cell layout) | 1, 2, 3, 4, 5 |
| Number of users (multi-cell layout) | 21 |
| Number of RIS elements, $N_{RIS}$ | 100, 400, 900, 1600 |

Table 5.1: Simulation parameters

The single-cell SU-MIMO scenarios are simulated extensively, i.e., for all the different simulation parameter values and the outcome of this simulation helped us to limit the interesting scenarios for other scenarios.

## 5.1 Single-cell SU-MIMO

In this section, we present the results for the three algorithms discussed in the previous section for the single-cell SU-MIMO scenario.

### 5.1.1 Effect of blocker strength

First, we present the performance of the three algorithms: benchmark, Algorithm 1, and 2 (as discussed in Chapter 4) as the value of the blocker strength, UBL, increases from 0 to 45 dB. Results for both indoor and outdoor users are shown in Figure 5.1. The left charts depict outcomes for outdoor users, while the right chart showcases results for indoor users. Each chart showcases a specific KPI on the y-axis, correlated with the blocker strength on the x-axis. In each chart, each curve represents one of the three proposed algorithms. Vertical lines in all the charts represent a 95% confidence interval for the given KPI in this and all the subsequent figures.

First, we look at the left chart, when all users are placed **outdoors**. We observe that *when blocker strength is 0 till 15 dB, the throughput plots remain the same for all three algorithms and the RIS-assigned ratio is zero* (Figures a-c)). Average cell throughput of constant 91.8 Mbps (which is equivalent to $0.8*R_{max}$, where $R_{max}$ was modeled (in Section 4.2.2) as the maximum achievable rate of 114.572 Mbps for a user at a given time TTI and 0.8 is the downlink TTIs to total TTIs ratio) is indicative of the fact that all the users of the cell in this particular scenario (outdoors, with up to 15 dB blocker) achieve a very strong cell-user link and is thus, are served with the maximum achievable data rate. Hence, RIS cannot improve on the throughput and is thus not optimized. *As the blocker strength increases further to 45 dB, we observe that the throughput curves (Figures a) and b)) reduce for the benchmark, and the RIS network usage increases (Figure c)).* As the RIS is now used for the users affected due to a blocker on the cell-user link, we observe that optimizing the RIS, using both Algorithms 1 and 2 improves both the average cell throughput and the $10^{th}$ throughput percentile as compared to the benchmark.

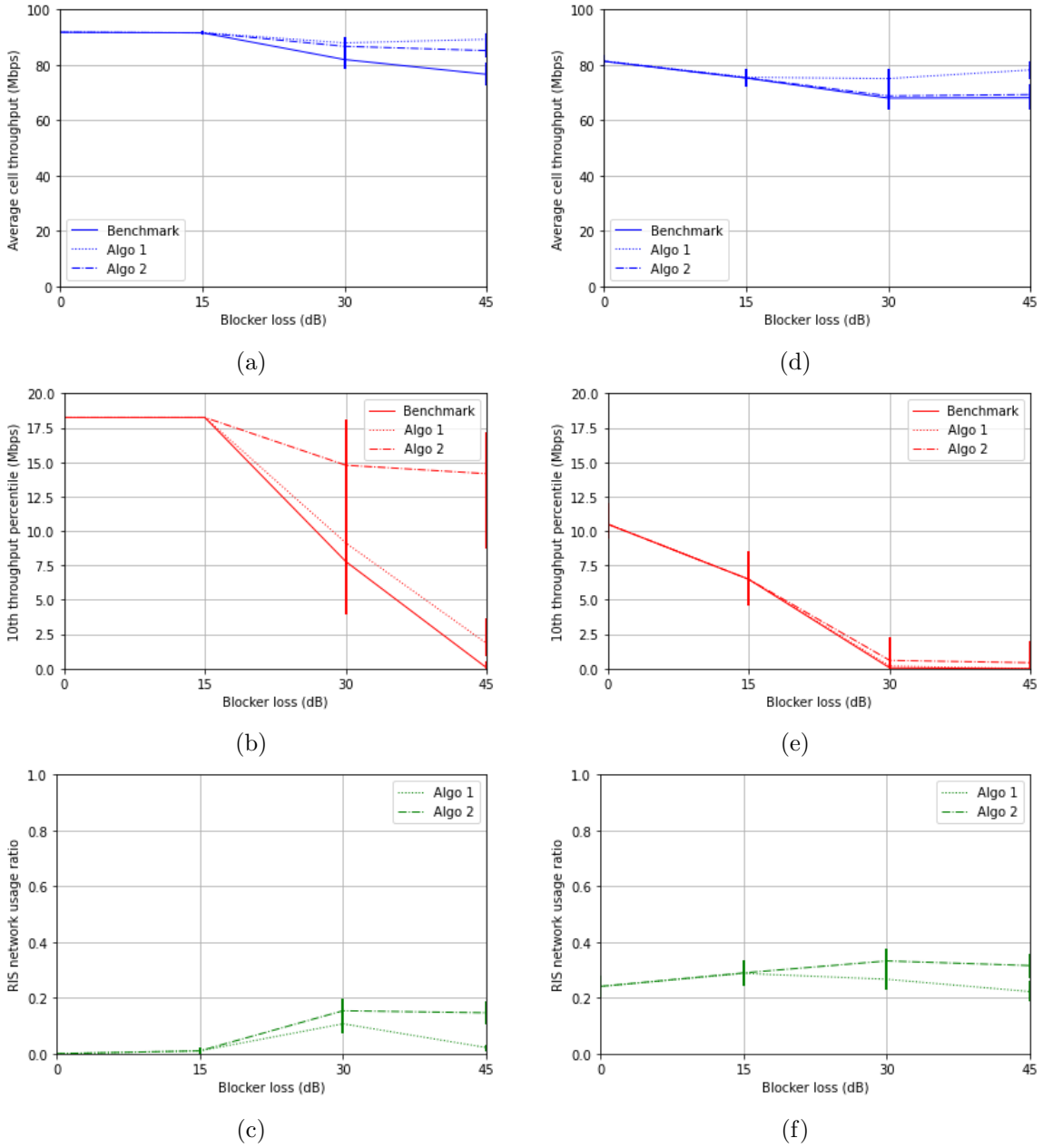


Figure 5.1: SCSU: Performance achieved by the three algorithms for outdoor users in a-c and for indoor users in d-f as blocker loss is varied

Next, we take a look at the right charts on the same figure where the users are placed **indoors** in the network. One distinguishing observation from these charts is that *RIS network usage is higher as compared to the outdoor users* (look at Figures c) and f)). Even when there is no blocker, (i.e. 0 dB blocker loss), RIS is being optimized for more than 20% of downlink slots. This could be understood from the fact that each indoor user experiences an additional building penetration loss (BPL) (refer to Section 3.4.1. This reduces the signal

strength at the user and provides the opportunity for the RIS to be used to improve the user throughputs. However, we observe from the top and middle right charts (Figures d) and e)), that *the gain achieved by optimizing RIS in algorithms 1 and 2 is not significant.* The signal strength from the indirect BS-RIS-UE path, after suffering BPL becomes very weak to add significant gain to the throughput. This makes RIS not useful for indoor users in a SC-SU-MIMO network.

We also observe from Figures 5.1 b) and e), that *Algorithm 2 outperforms both the benchmark and Algorithm 1, in terms of* $10^{th}$ *throughput percentile.* This makes sense as Algorithm 2 enables RIS-aware proportional fairness-based scheduling. As the benefit from the RIS is considered during scheduling, users that may benefit from RIS are scheduled more often as compared to Algorithm 1 (refer to Figure c)), and thus, the network experiences better $10^{th}$ throughput percentile. However, we also observe from the top two charts that *Algorithm 1 outperforms Algorithm 2 in terms of average cell throughput.* On closer inspection, we describe this as the limitation in the design of Algorithm 1. Though, Algorithm 1 works also on proportional fairness-based scheduling, it is actually unfair in nature. Let's look again at the proportional fairness scheduler as described in Equation 4.12. Here, though the estimated data rate (in the numerator) does not consider RIS, the average data rate (in the denominator) considers the benefit of RIS. Thus, the users that have benefited from RIS will now be served even less as the estimated data rate for them is still quite low while the denominator is high, making the PF index to be smaller. This results in users that have already higher data rate being served more often and thus increasing the average cell throughput. This also explains why the RIS network usage ratio reduces after a threshold blocker strength and correspondingly, average cell throughput starts increasing for Algorithm 1.

From the discussion above, we can draw out the key conclusions of this section as 1) RIS is most useful in the outdoor scenario when the blocker strength is high, 2) RIS does not prove useful for indoor users in this scenario of SC-SU-MIMO, and 3) Algorithm 2 outperforms the benchmark in terms of cell throughput and $10^{th}$ throughput percentile and is also much more fair as compared to the Algorithm 1.

### 5.1.2 Effect of blocker probability

Having discussed how the blocker strength in combination with the user type has an impact on the throughput metrics and the RIS network usage of all three algorithms, we now wish to see how the results may vary if the blocker probability is changed to 10%. We see the results in Figure 5.2

Comparing 5.1 and 5.2, we see that all the trends as discussed before remain the same. Since the blocker probability is lower now. the impact of RIS should also be lower and this is visible by the reduced RIS network usage and the smaller improvement in the throughput metrics.

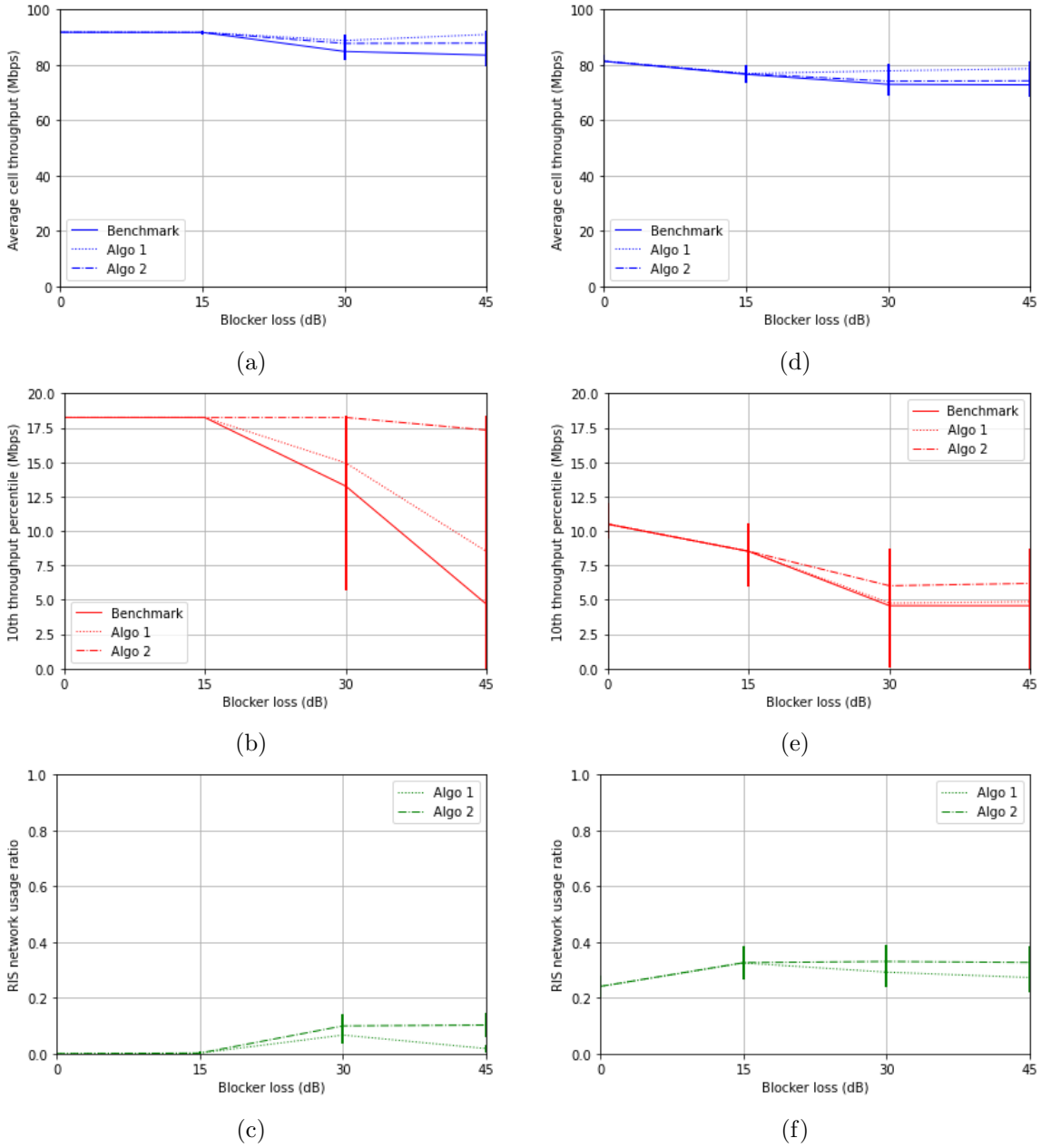


Figure 5.2: SCSU: Performance achieved by the three algorithms for outdoor users in a-c and for indoor users in d-f as blocker loss is varied when $P_{BL} = 0.1$.

### 5.1.3 Effect of RIS deployment position

Next, we wish to see the impact of the deployment position of RIS between A, B, and C on the performance of the three algorithms. Since we do not observe gain by RIS for indoor users in single-cell SU-MIMO scenarios, we limit this discussion to the case with outdoor users. Results for the same are shown in Figure 5.3.

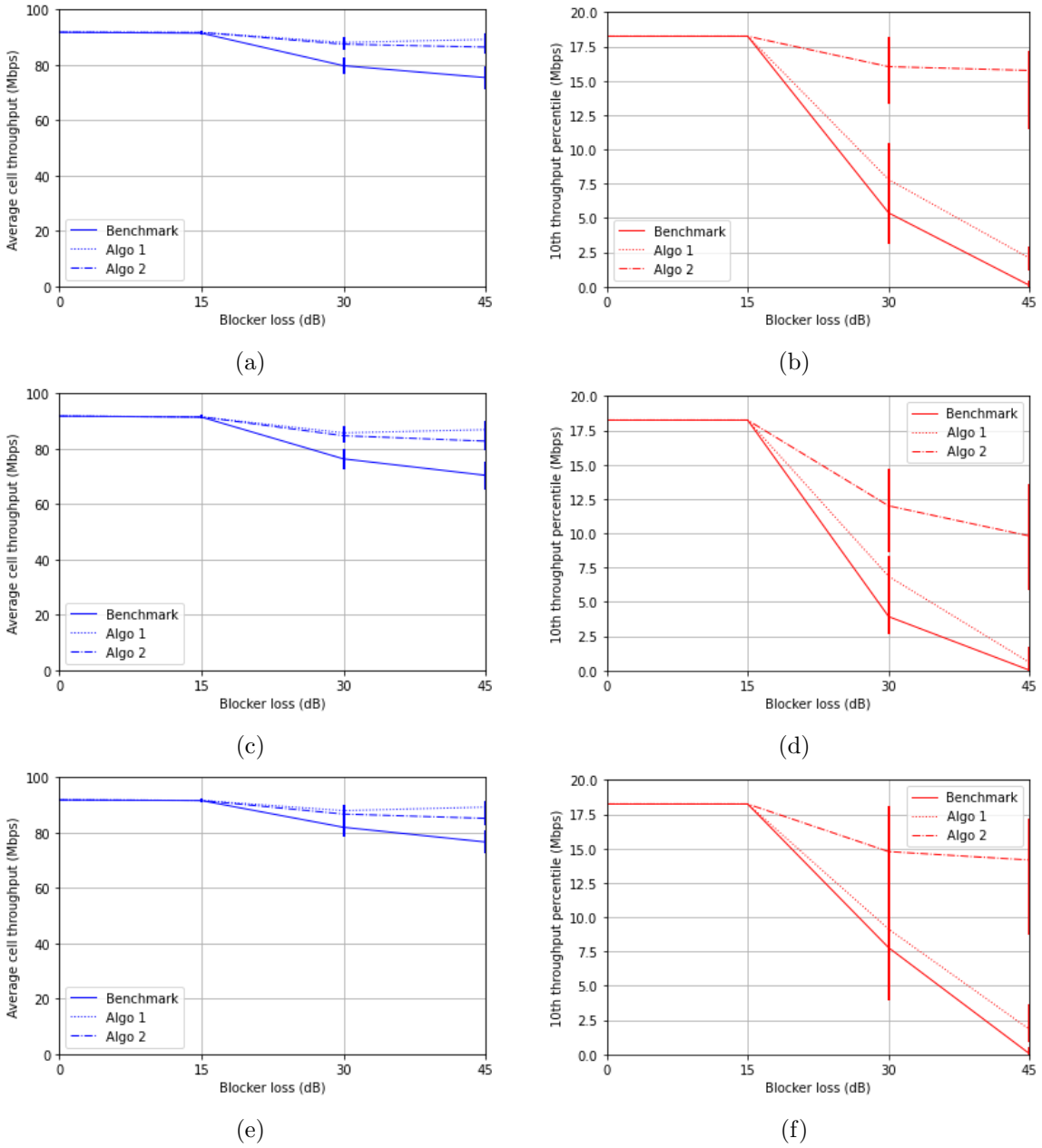


Figure 5.3: SCSU: Performance achieved by the three algorithms for outdoor users for RIS deployment position A in a-b, deployment position B in c-d, and for RIS deployment position C in e-f.

An interesting observation from this figure is that *all three RIS deployments have quite similar throughput plots*. The reason for this is the trade-off between reducing cell-RIS path loss to the number of users that may benefit from a given RIS position.

Another interesting observation is that *for the RIS deployment C, even the benchmark has*

*better performance than other algorithms.* This can be explained due to the high signal strength achieved by the users, (even with non-optimized RIS) due to an improved cell-RIS link and thus, a better indirect path.

Since this discussion is inconclusive in proving the best RIS deployment position among the three, we chose arbitrarily RIS deployment position C to be the default setting in the next discussion based solely on the best $10^{th}$ throughput percentile among all at 30 dB locker strength.

### 5.1.4 Effect of number of RIS elements

Now, we wish to study the impact of the number of RIS elements on the performance of the three algorithms. These results are presented in Figure 5.4.

On the left chart, we plot the results when the blocker loss is kept at the default setting of 30 dB. However, due to most users experiencing maximum data, we are unable to observe the trend as the number of RIS elements varies. Thus, on the right chart, we plot results when blocker loss is 45 dB. From Figure 5.4 d) and e), we see that the performance of both algorithms 1 and 2 increases as the number of RIS elements increases. Intuitively, increasing the number of RIS elements increases the captured energy and the focusing capability of the RIS, thus providing a better indirect path. One interesting observation is *that increasing the number of RIS elements, not only increases the cell throughput but also the* $10^{th}$ *throughput percentile* when using Algorithm 2. As users are served better with RIS, they are served more, which makes the network decisions more fair.

### 5.1.5 Effect of number of users

Lastly, we analyse the impact of the number of users in a cell on the performance of the three algorithms when a RIS is present. These results are presented in figure 5.5.

From Figure 5.5, we observe the expected decrease in the $10^{th}$ throughput percentile and the expected increase in cell throughput for the benchmark as the number of users increases. We observe no impact on RIS network usage as the number of users varies. Thus, considering Algorithms 1 and 2, *RIS is not affected by the number of users in a cell.* This especially makes sense in this scenario when there is no intra or inter-cell interference due to additional users. Further, since only one user is scheduled at a time, RIS is not affected by how many users are active in total.

In this section, we described in detail the results obtained for single-cell SU-MIMO. Let us summarize the key observations from this section before we move on to explore the single-cell MU-MIMO scenario:

1. Blocker probability, blocker strength, and user type together decide the performance in a RIS-aided network. Outdoor users with high blocker strength and high blocker probability have the best improvement with RIS as compared to the benchmark of not using RIS.

2. RIS deployment position does not play a key role in the SC-SU-MIMO scenario.

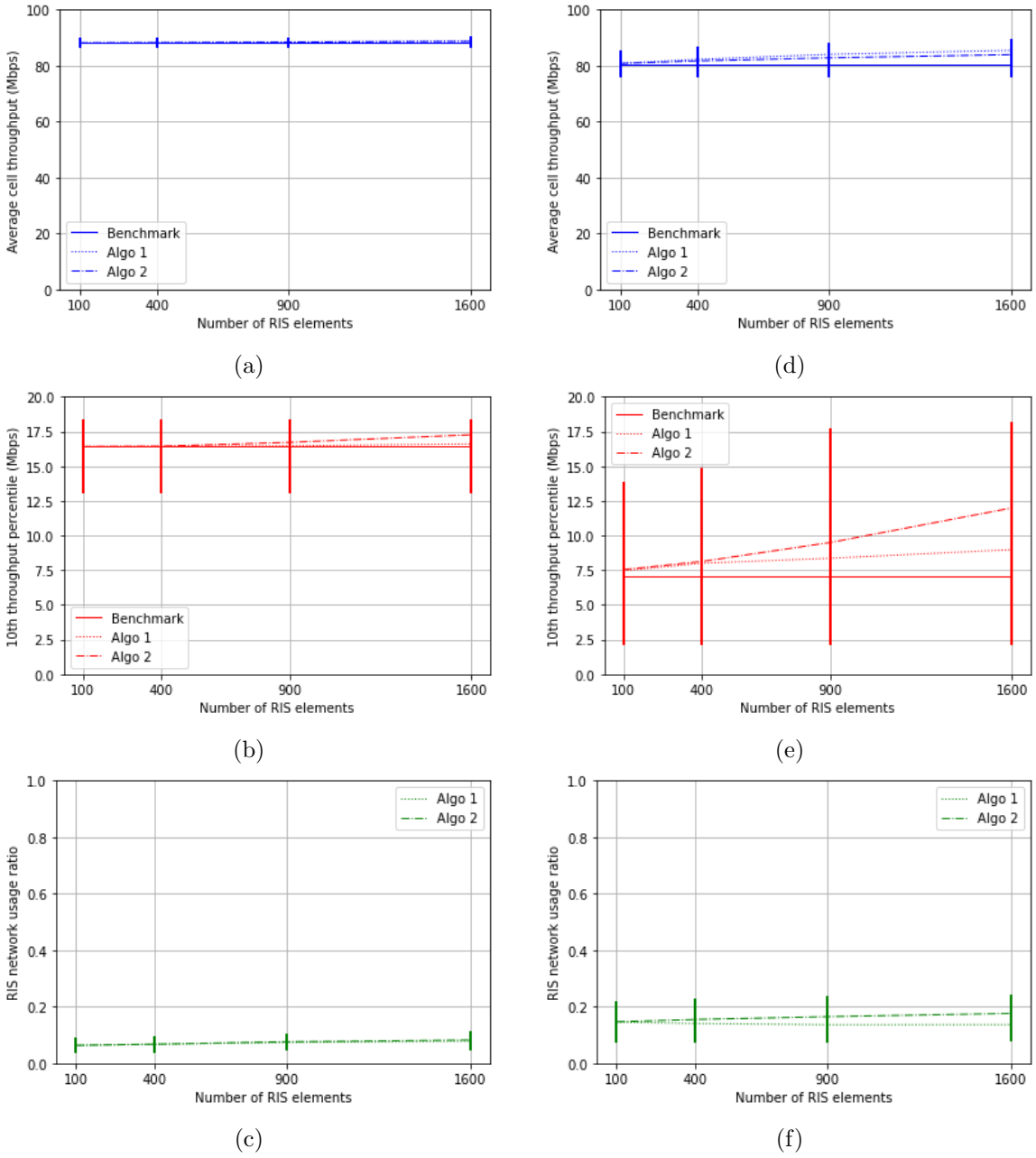


Figure 5.4: SCSU: Performance achieved by the three algorithms as the number of RIS elements are varied when blocker loss is 30 dB in a-c and 45 dB in d-f

3. Algorithm 2 outperforms both the benchmark and Algorithm 1 in terms of $10^{th}$ throughput percentile.

4. Increasing the number of RIS elements improves both the average cell throughput and $10^{th}$ throughput percentile for algorithm 2.

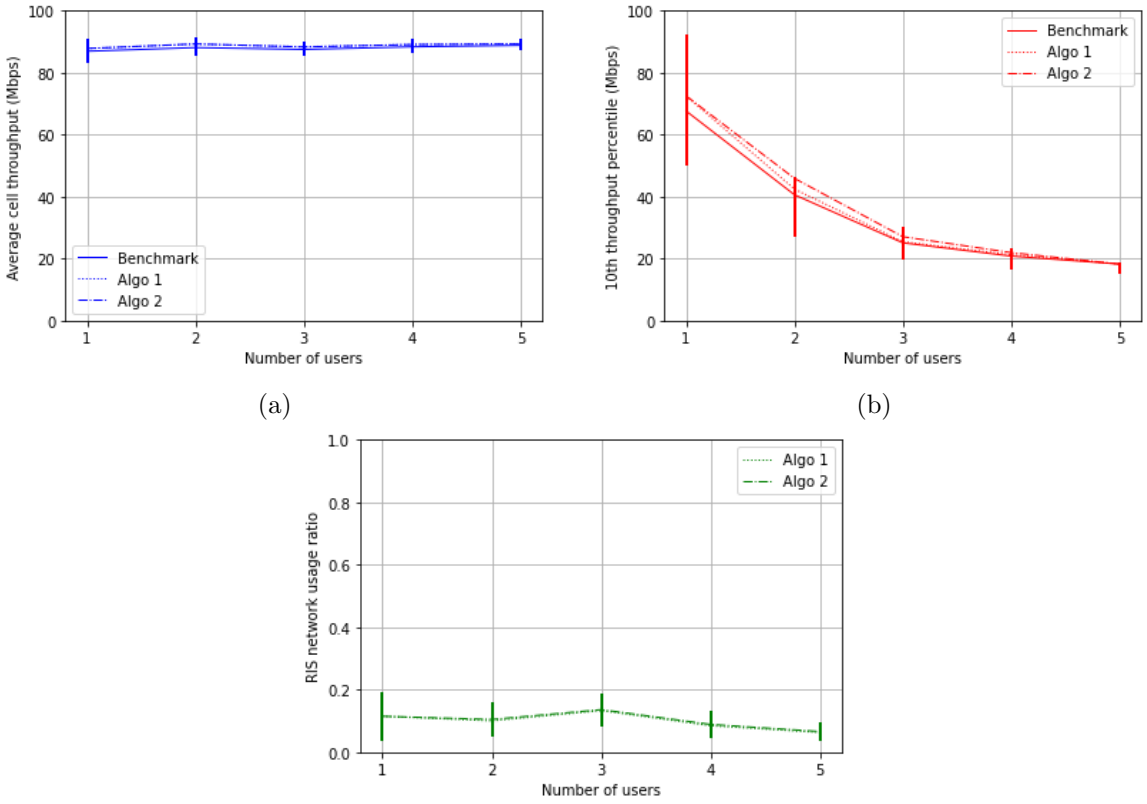


(a) (b)

(c)

Figure 5.5: SCSU: Performance achieved by the three algorithms as the number of users is varied.

Since, we do not expect the impact of blocker probability, RIS deployment position, or the number of RIS elements to be any different than the SC-SU-MIMO, we skip that analysis from now onwards. An interested reader may look at Appendix B to observe detailed results for these scenarios. We now fix the value of blocker probability to be 0.2, RIS deployment to be C, and $N_{RIS}$ to be 1600.

## 5.2 Single-cell MU-MIMO

This section discusses the results of a single-cell MU-MIMO scenario. We are interested in seeing how the multi-user scheduling and hence, the addition of intra-cell interference may affect the throughput performance of the three algorithms.

### 5.2.1 Effect of blocker strength

Let us start with how the blocker strength may impact the performance of the three proposed algorithms for outdoor and indoor users. We observe these results in Figure 5.6. Note that we have increased the limits of the y-axis for throughput plots.

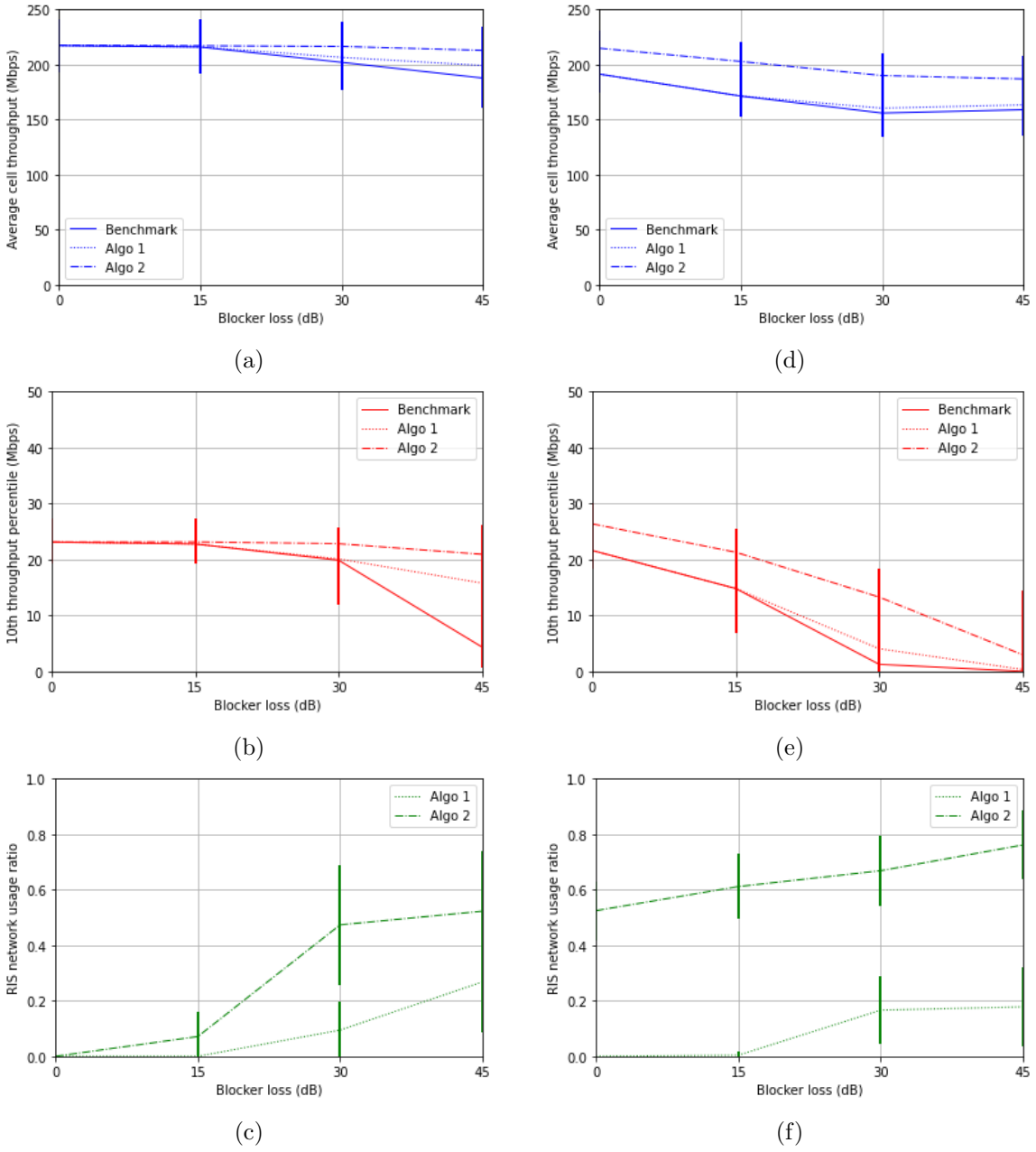


Figure 5.6: SCMU: Performance achieved by the three algorithms for outdoor users in a-c and for indoor users in d-f as blocker loss varies.

Compared to the last scenario of SC-MU-MIMO, we see two main differences. Firstly, we observe *a significant gain for indoor users with Algorithm 2 even when there is no blocker*. This is explained by the fact that now more users are scheduled at the given time. So, the RIS network ratio is much higher which results in any users that may benefit from RIS being scheduled more often, hence, improving the average cell throughput.

Secondly, we observe that now, *Algorithm 2 outperforms both the benchmark and Algorithm 1 in all the metrics*. Let us try to understand this by reviewing how Algorithm 1 works. In this algorithm, first, the users are independently scheduled and then the RIS is used if it can improve any performance. Note that in the case of MU-MIMO, as RIS is optimized, the orthogonality for the co-scheduled users needs to be satisfied with the updated channel. This condition is difficult to match and thus, the RIS network usage is much smaller with Algorithm 1 as compared to Algorithm 2, leading to lower throughputs as well.

### 5.2.2 Effect of number of users

Next, we wish to see the impact of the number of users on the performance of three algorithms. We can observe from Figure 5.7 that the RIS network usage ratio almost linearly increases with the number of users (Figure c)). This shows as more users are present in the network, more users are co-scheduled, and thus, the RIS is being used more often. Thus, not only does the cell throughput increase with the number of users (refer to Figure a)), but the performance gain from Algorithm 1 and 2 as compared to the benchmark also increases (Figures a) and b)).

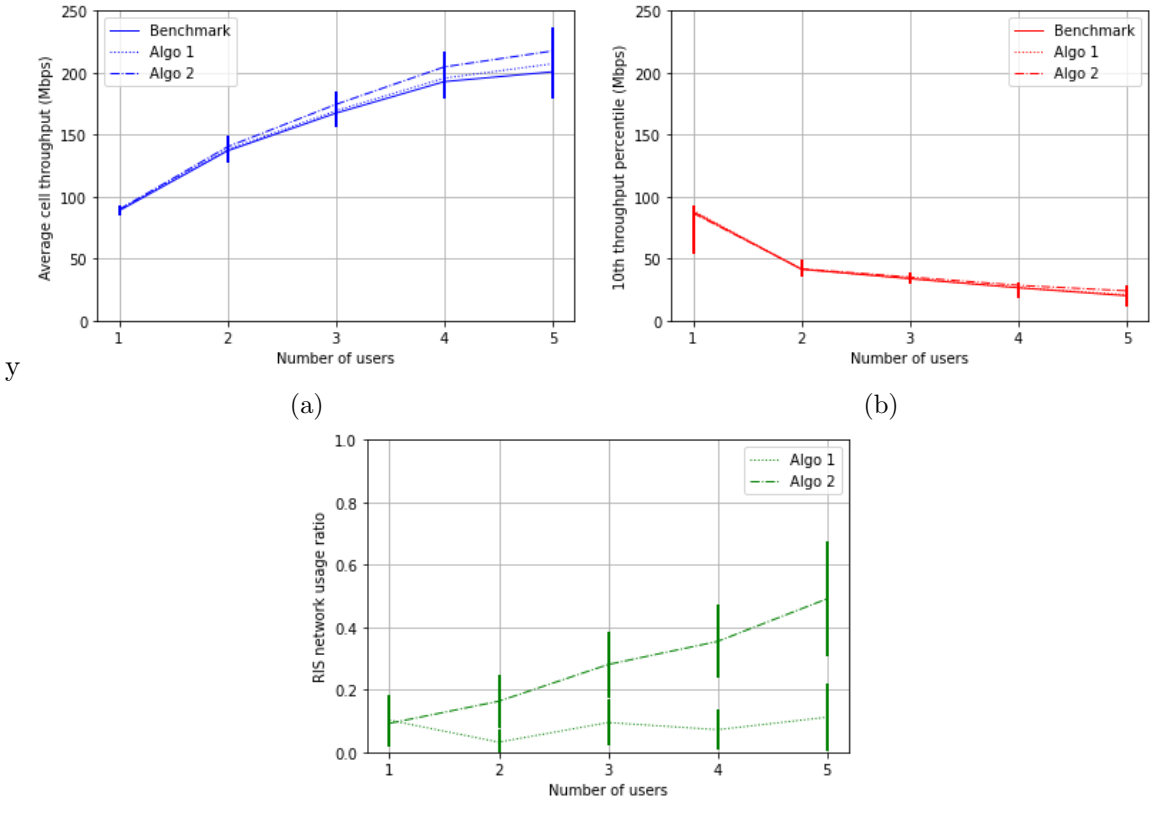


y

(a) (b)

(c)

Figure 5.7: SCMU: Performance achieved by the three algorithms for outdoor users as the number of users varies.

The key insight for the results obtained for SC-MU-MIMO is that though RIS may not prove useful in a single-cell SU-MIMO case for indoor users, it clearly improves the throughput in a single-cell MU-MIMO case, even with no blocker present. Furthermore, in the case of MU-MIMO, it is important to jointly optimize scheduling with RIS since that proves to have the best performance for all the defined metrics.

## 5.3 Multi-cell SU-MIMO

Till now, we discussed a single-cell scenario where users are constrained to be associated with only one cell. This has also resulted in no inter-cell interference. Now, in this section, we aim to see how the performance of the three algorithms would vary in a multi-cell scenario.

Here, we first consider a SU-MIMO and present results for the metrics defined for the users of the innermost cell, cell 0 in Figure 5.8.

Interestingly, we see *no improvement in throughput* when RIS is used, as compared to the benchmark. This is explained by the fact that when the user of the innermost cell is blocked on the cell-user link and thus, has a weak path, it gets associated with another cell. Since we have constrained the RIS to be used by the users of the innermost cell, these users then no longer benefit from RIS. In the case of indoor users with weak path loss, even when they get optimized for RIS (look at Figure f)), we do not see any visible improvement (Figures d) and e)) due to building penetration loss for the indoor users and high inter-cell interference.

Thus, we can conclude that under the conditions defined by our multi-cell scenario, the given algorithms are not useful and RIS does not improve the throughput in SU-MIMO. Another way to look is that, in the case of a multi-cell scenario, it may be useful to consider RIS-aware cell-UE association decisions in future work.

## 5.4 Multi-cell MU-MIMO

We finally present the results for the multi-cell MU-MIMO scenario in Figure 5.9. We have removed Algorithm 1 from this analysis as we already proved that it does not improve any performance in a MU-MIMO case, and even if it does, it is at the expense of fairness.

We observe from Figures 5.9 a-b,d-e that the Algorithm 2 outperforms the benchmark. Considering the previous discussion of MC-SU-MIMO, this seems rather counter-intuitive as we concluded that the users with high blockers on the direct cell-user path are simply associated with another cell. That still holds true in this discussion. It is still only the users with weak path loss that are associated with the RIS. But, we observe from the bottom two figures that the RIS network usage is high, which enables all the users to be scheduled much more often and because of this high RIS network usage ratio, we observe performance gains in the throughput KPIs.

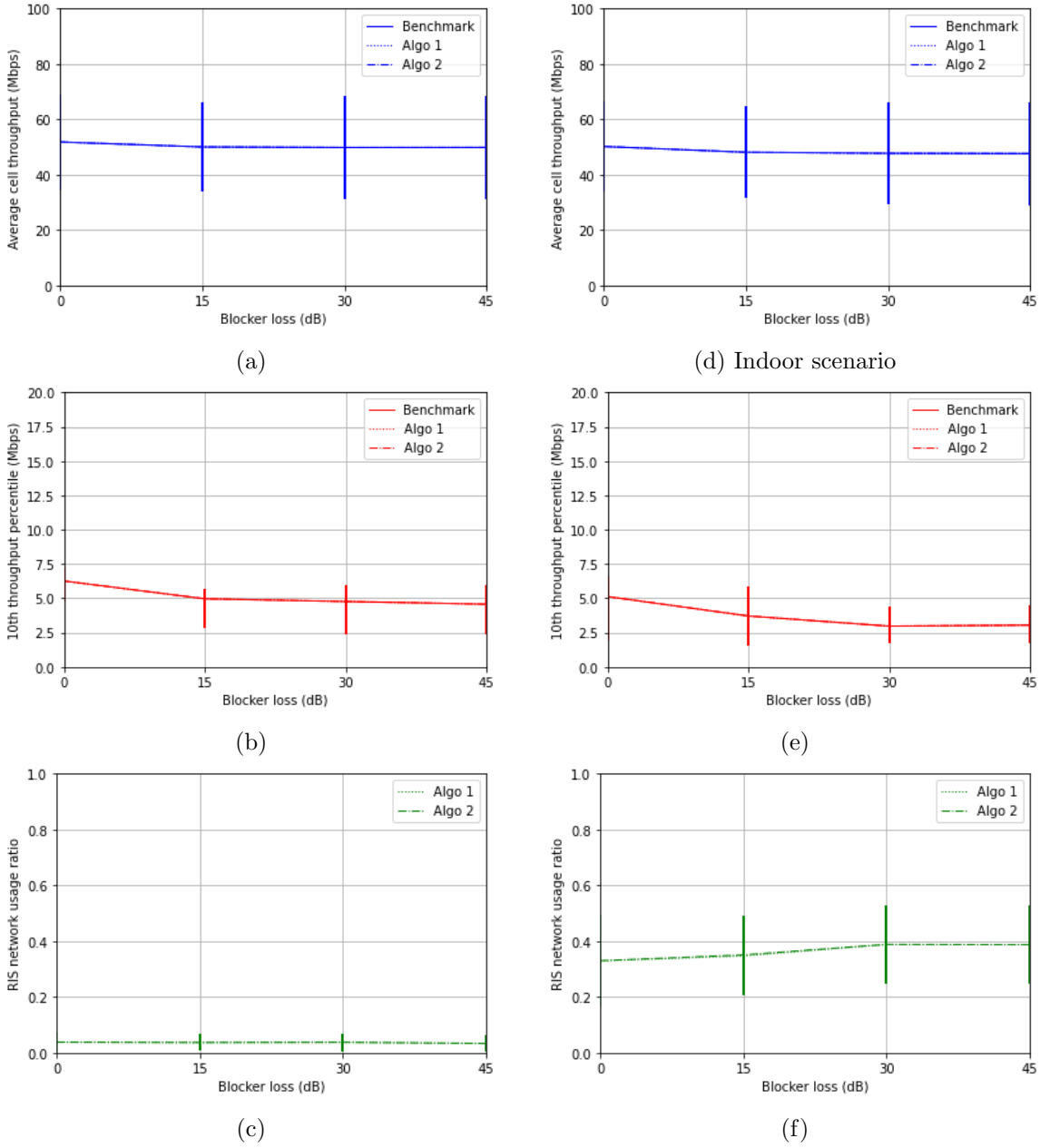


Figure 5.8: MCSU: Performance achieved by the three algorithms for outdoor users in a-c and for indoor users in d-f as blocker loss varies.

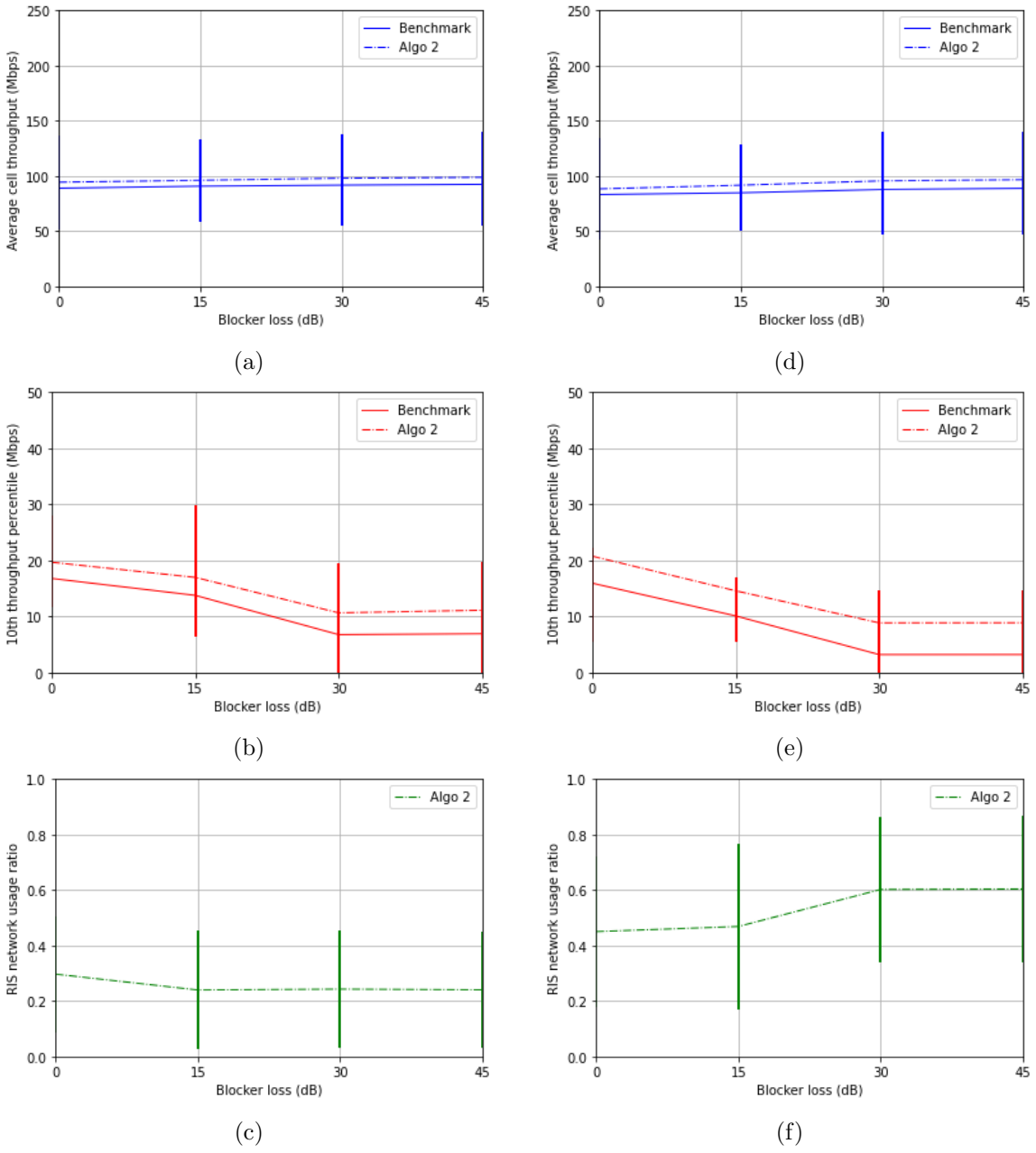


Figure 5.9: MCMU: Performance achieved by the three algorithms for outdoor users in a-c and for indoor users in d-f as blocker loss varies.

# Chapter 6

# Conclusion

In this study, we introduce three algorithms aimed at optimizing radio resource management tasks in a 6G-enabled network. We conducted a comparative analysis of these algorithms in terms of performance among themselves, as well as against various scenarios. Our simulations encompassed both single-cell and multi-cell configurations, incorporating both single-user and multi-user scheduling. Additionally, we evaluated performance under distinct conditions, including user placement, blocker strength, blocker probability, and RIS deployment positions.

To achieve our objective, we commenced with modeling the network, its components, and the channel within a RIS-augmented framework. We outlined the methods employed for SINR and throughput calculations. Subsequently, we explained the three algorithmic solutions for radio resource management tasks in detail. Lastly, we analyzed the comprehensive simulation results across various scenarios.

The subsequent section presents a concise summary of our conclusions. We end this chapter by acknowledging the limitations of this thesis and identifying future avenues to extend this research.

## 6.1 Summary

Our findings reveal that Algorithm 2, that optimizes RIS-aware scheduling, RIS configuration matrix, and precoding matrix at the cell, consistently outperforms the benchmark, both in terms of average cell throughput and the $10^{th}$ throughput percentile. It also surpasses Algorithm 1, which undertakes independent scheduling without considering RIS, in most scenarios—except for SC-SU-MIMO, where Algorithm 2's fairness superiority is evident.

Considering the objective of optimal RIS application, we draw the following conclusions:

- For SC-SU-MIMO, RIS deployment is beneficial solely for outdoor users experiencing substantial blocker losses on the cell-user link. With a 30 dB blocker, Algorithm 2 enhances the $10^{th}$ throughput percentile to twice the benchmark.

- For SC-MU-MIMO, RIS deployment proves advantageous for both indoor and outdoor users. Multi-user scheduling enables RIS usage in up to 78% of downlink slots, improving the $10^{th}$ throughput percentile by 14.8% for indoor users with 30 dB blocker. In the context of MU-MIMO, where scheduling hinges on channel conditions, RIS consideration during scheduling becomes vital to maximize potential benefits.
- For MC-SU-MIMO, within the existing simulation setup and proposed algorithms, RIS deployment does not yield any network advantage.
- For MC-MU-MIMO, RIS deployment remains advantageous for both indoor and outdoor users. Multi-user scheduling permits RIS utilization in up to 60% of downlink slots for the indoor users, leading to a 32.1% enhancement in the $10^{th}$ throughput percentile for the indoor users with 30 dB blocker loss.
- The trend in RIS deployment strategies across different RIS locations remains consistent, albeit requiring more intricate analysis due to the inherent trade-off between cell-RIS distance and the number of beneficiaries.
- In MU-MIMO, the number of users in the network significantly influences the performance gain.
- RIS usefulness escalates with heightened blocker probability and/or increased blocker strength.
- An increase in the number of RIS elements directly correlates to throughput improvement (both cell and user $10^{th}$ throughput percentile).

## 6.2 Future work

Throughout this study, we've identified several potential research directions to extend the work presented in this thesis:

- While our study encompassed radio resource management tasks such as RIS-UE association, user scheduling, and beamforming, an examination of BS-UE association could further enhance the understanding, particularly in a multi-cell layout.
- A discussion pertaining to coverage was omitted in this thesis. Addressing scenarios with high blockers where numerous users might be out of coverage and assessing the potential for RIS improvement would be insightful.
- Although our study employed heuristic algorithms, exploring advanced AI-based solutions could enhance both performance and computational feasibility.
- We operated under the assumption of perfect Channel State Information (CSI). Addressing the impact of realistic CSI and developing efficient CSI acquisition algorithms that complement radio resource management tasks are worthwhile avenues for future exploration.

# Bibliography


[1] S. Basharat, M. Khan, M. Iqbal, U. Hashmi, S. A. R. Zaidi, and I. Robertson, "Exploring Reconfigurable Intelligent Surfaces for 6G: State-of-the-Art and the Road Ahead," *IET Communications*, vol. 16, 08 2022.

[2] K. Brueninghaus, D. Astely, T. Salzer, S. Visuri, A. Alexiou, S. Karger, and G.-A. Seraji, "Link performance models for system level simulations of broadband radio access systems," in *2005 IEEE 16th International Symposium on Personal, Indoor and Mobile Radio Communications*, vol. 4, 2005.

[3] J. Zuo, Y. Liu, E. Basar, and O. A. Dobre, "Intelligent Reflecting Surface Enhanced Millimeter-Wave NOMA Systems," *IEEE Communications Letters*, vol. 24, no. 11, 2020.

[4] Y. Chen, Y. Wang, J. , and Z. Li, "Resource Allocation for Intelligent Reflecting Surface Aided Vehicular Communications," *IEEE Transactions on Vehicular Technology*, vol. 69, no. 10, 2020.

[5] X. Yu, D. Xu, Y. Sun, D. W. K. Ng, and R. Schober, "Robust and Secure Wireless Communications via Intelligent Reflecting Surfaces," *IEEE Journal on Selected Areas in Communications*, vol. 38, no. 11, 2020.

[6] C. Pan, H. Ren, K. Wang, M. Elkashlan, A. Nallanathan, J. Wang, and L. Hanzo, "Intelligent Reflecting Surface Aided MIMO Broadcasting for Simultaneous Wireless Information and Power Transfer," *IEEE Journal on Selected Areas in Communications*, vol. 38, no. 8, 2020.

[7] C. Huang, A. Zappone, G. C. Alexandropoulos, M. Debbah, and C. Yuen, "Reconfigurable Intelligent Surfaces for Energy Efficiency in Wireless Communication," *IEEE Transactions on Wireless Communications*, vol. 18, no. 8, 2019.

[8] S. Zeng, H. , B. Di, Z. Han, and L. Song, "Reconfigurable Intelligent Surface (RIS) Assisted Wireless Coverage Extension: RIS Orientation and Location Optimization," *IEEE Communications Letters*, vol. 25, no. 1, 2021.

[9] S. and R. , "Intelligent Reflecting Surface Aided Multi-User Communication: Capacity Region and Deployment Strategy," *IEEE Transactions on Communications*, vol. 69, no. 9, 2021.

[10] Q. Wu and R. , "Intelligent Reflecting Surface Enhanced Wireless Network via Joint Active and Passive Beamforming," *IEEE Transactions on Wireless Communications*, vol. 18, no. 11, 2019.

[11] X. Yu, D. Xu, and R. Schober, "MISO Wireless Communication Systems via Intelligent Reflecting Surfaces," in *2019 IEEE/CIC International Conference on Communications in China (ICCC)*, 2019.

[12] C. Huang, R. Mo, and C. Yuen, "Reconfigurable Intelligent Surface Assisted Multiuser MISO Systems Exploiting Deep Reinforcement Learning," *IEEE Journal on Selected Areas in Communications*, vol. 38, no. 8, 2020.

[13] C. Huang, G. C. Alexandropoulos, C. Yuen, and M. Debbah, "Indoor Signal Focusing with Deep Learning Designed Reconfigurable Intelligent Surfaces," in *2019 IEEE 20th International Workshop on Signal Processing Advances in Wireless Communications (SPAWC)*, 2019.

[14] Z. Zhang, T. Jiang, and W. Yu, "User Scheduling Using Graph Neural Networks for Reconfigurable Intelligent Surface Assisted Multiuser Downlink Communications," in *2022 IEEE International Conference on Acoustics, Speech and Signal Processing (ICASSP)*, 2022.

[15] Y. Zhu, M. Li, Y. Liu, Q. Liu, Z. Chang, and Y. Hu, "DRL-based Joint Beamforming and BS-RIS-UE Association Design for RIS-Assisted mmWave Networks," in *2022 IEEE Wireless Communications and Networking Conference (WCNC)*, 2022.

[16] T. Yoo and A. Goldsmith, "On the optimality of multiantenna broadcast scheduling using zero-forcing beamforming," *IEEE Journal on Selected Areas in Communications*, vol. 24, no. 3, 2006.

[17] A. Wiesel, Y. C. Eldar, and S. Shamai, "Zero-Forcing Precoding and Generalized Inverses," *IEEE Transactions on Signal Processing*, vol. 56, no. 9, 2008.

[18] 3GPP, "Study on channel model for frequencies from 0.5 to 100 GHz," 3GPP Technical Specification Group Radio Access Network, Technical Report TR38.901, 2019.

[19] F. Gunnarsson, M. N. Johansson, A. Furuskar, M. Lundevall, A. Simonsson, C. Tidestav, and M. Blomgren, "Downtilted Base Station Antennas - A Simulation Model Proposal and Impact on HSPA and LTE Performance," in *2008 IEEE 68th Vehicular Technology Conference*, 2008.

[20] T.-H. Vu and S. Kim, "Performance Analysis of Full-Duplex Two-Way RIS-Based Systems With Imperfect CSI and Discrete Phase-Shift Design," *IEEE Communications Letters*, vol. 27, no. 2, 2023.

[21] W. Tang, M. Z. Chen, X. Chen, J. Y. Dai, Y. Han, M. Di Renzo, Y. Zeng, S. Jin, Q. Cheng, and T. J. Cui, "Wireless Communications With Reconfigurable Intelligent Surface: Path Loss Modeling and Experimental Measurement," *IEEE Transactions on Wireless Communications*, vol. 20, no. 1, 2021.

[22] H. Friis, "A Note on a Simple Transmission Formula," *Proceedings of the IRE*, vol. 34, no. 5, 1946.

[23] R. Fraile, J. F. Monserrat, J. Gozálvez, and N. Cardona, "Mobile radio bi-dimensional large-scale fading modelling with site-to-site cross-correlation," *Eur. Trans. Telecommun.*, vol. 19, no. 1, 2008.

[24] Z. Lai, N. Bessis, G. Roche, P. Kuonen, J. , and G. Clapworthy, "The Characterisation of Human Body Influence on Indoor 3.5 GHz Path Loss Measurement," 2010.

[25] S. Jaeckel, L. Raschkowski, K. Börner, L. Thiele, F. Burkhardt, and E. Eberlein, "QuaDRiGa-Quasi Deterministic Radio Channel Generator, User Manual and Documentation," Fraunhofer Heinrich Hertz Institute, Tech. Rep. v1.2.3-307, 2014.

[26] 3GPP, "NR; Physical layer procedures for data," 3GPP Technical Specification Group Radio Access Network, Technical Report TS38.214, 2023.

[27] P. Mogensen, W. Na, I. Z. Kovacs, F. Frederiksen, A. Pokhariyal, K. I. Pedersen, T. Kolding, K. Hugl, and M. Kuusela, "LTE Capacity Compared to the Shannon Bound," in *2007 IEEE 65th Vehicular Technology Conference*, 2007.

[28] A. V. Oppenheim and R. W. Schafer, *Digital Signal Processing.* Upper Saddle River, NJ: Pearson, 1975.

# Appendix A

# Extensive set of results

Below we provide the set of results excluded from the thesis.

## A.1 SC-SU MIMO

Figure A.1 provides the counterpart of Figure5.3 by providing results for indoor users.

## A.2 SC-MU-MIMO

Figure A.2 provides the effect of RIS dployment on outdoor users in SC-MU-MIMO scenario.

Figure A.3 provides the effect of RIS dployment on indoor users in SC-MU-MIMO scenario.

## A.3 MC-SU-MIMO

Figure A.4 provides the effect of RIS dployment on outdoor users in MC-SU-MIMO scenario.

Figure A.5 provides the effect of RIS dployment on indoor users in MC-SU-MIMO scenario.

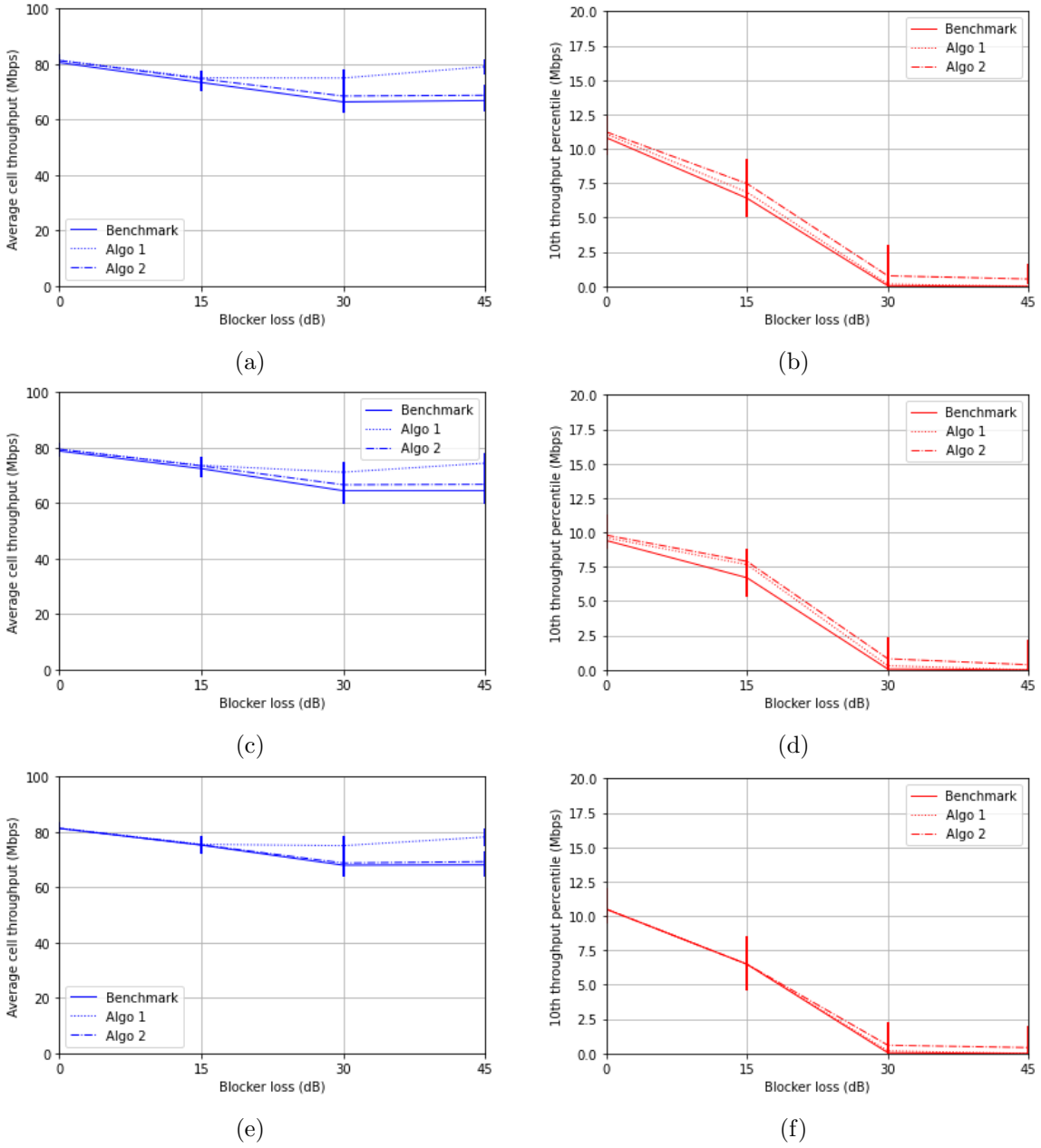


Figure A.1: SCSU: Performance achieved by the three algorithms for indoor users for RIS deployment position A in a-b, deployment position B in c-d, and for RIS deployment position C in e-f.

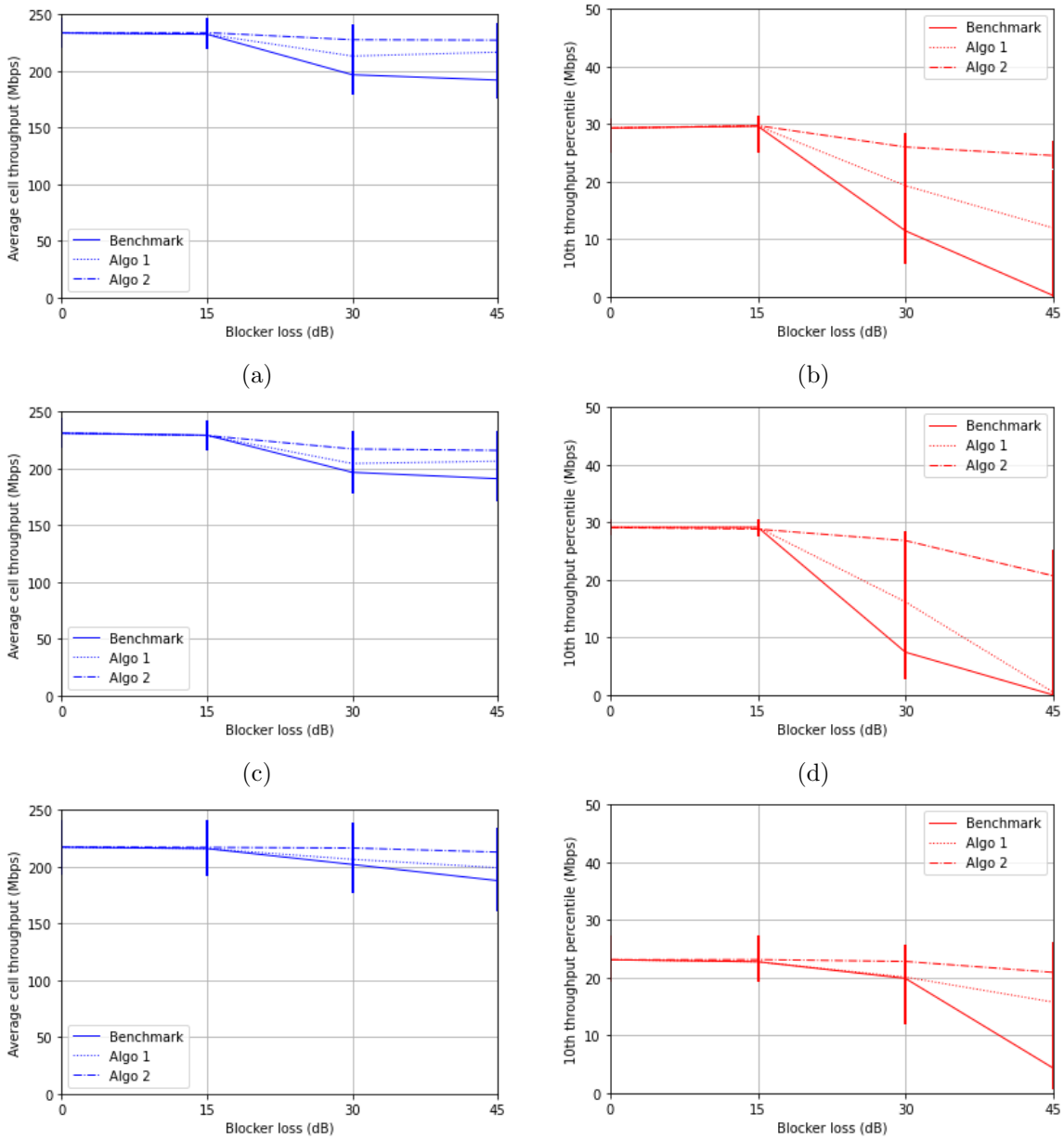


Figure A.2: SCMU: Performance achieved by the three algorithms for outdoor users for RIS deployment position A in a-b, deployment position B in c-d, and for RIS deployment position C in e-f.

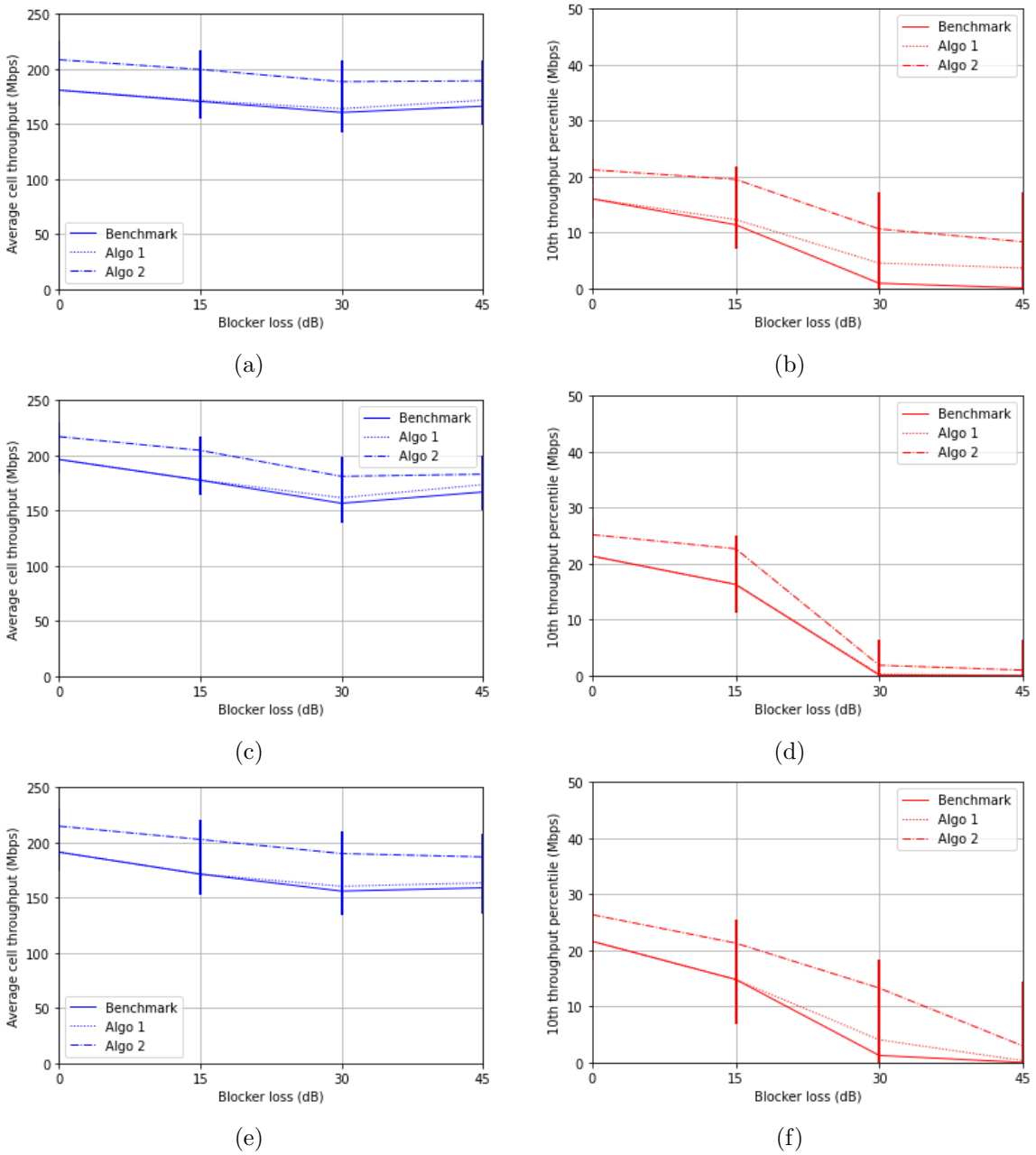


Figure A.3: SCMU: Performance achieved by the three algorithms for indoor users for RIS deployment position A in a-b, deployment position B in c-d, and for RIS deployment position C in e-f.

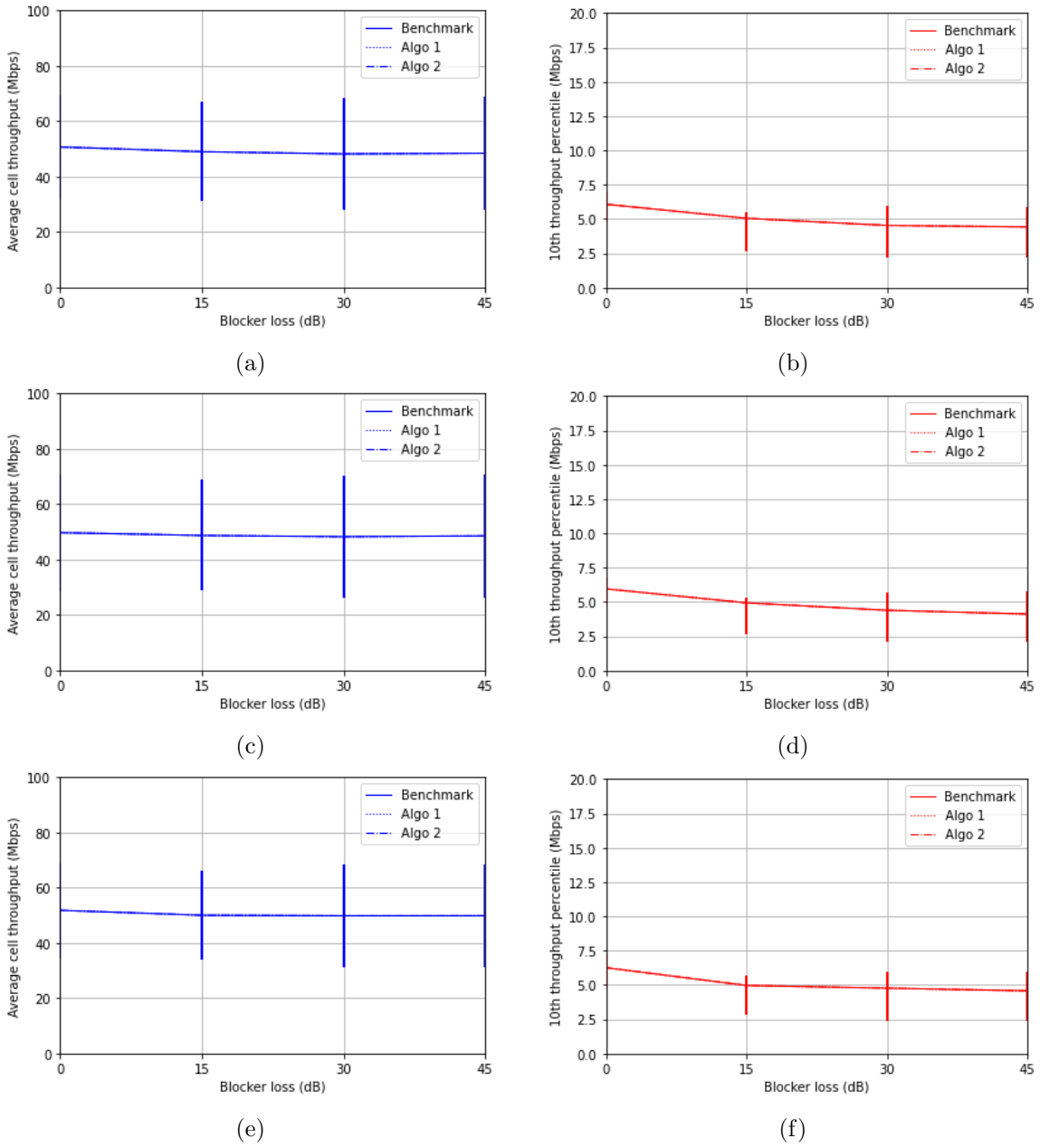


Figure A.4: MCSU: Performance achieved by the three algorithms for outdoor users for RIS deployment position A in a-b, deployment position B in c-d, and for RIS deployment position C in e-f.

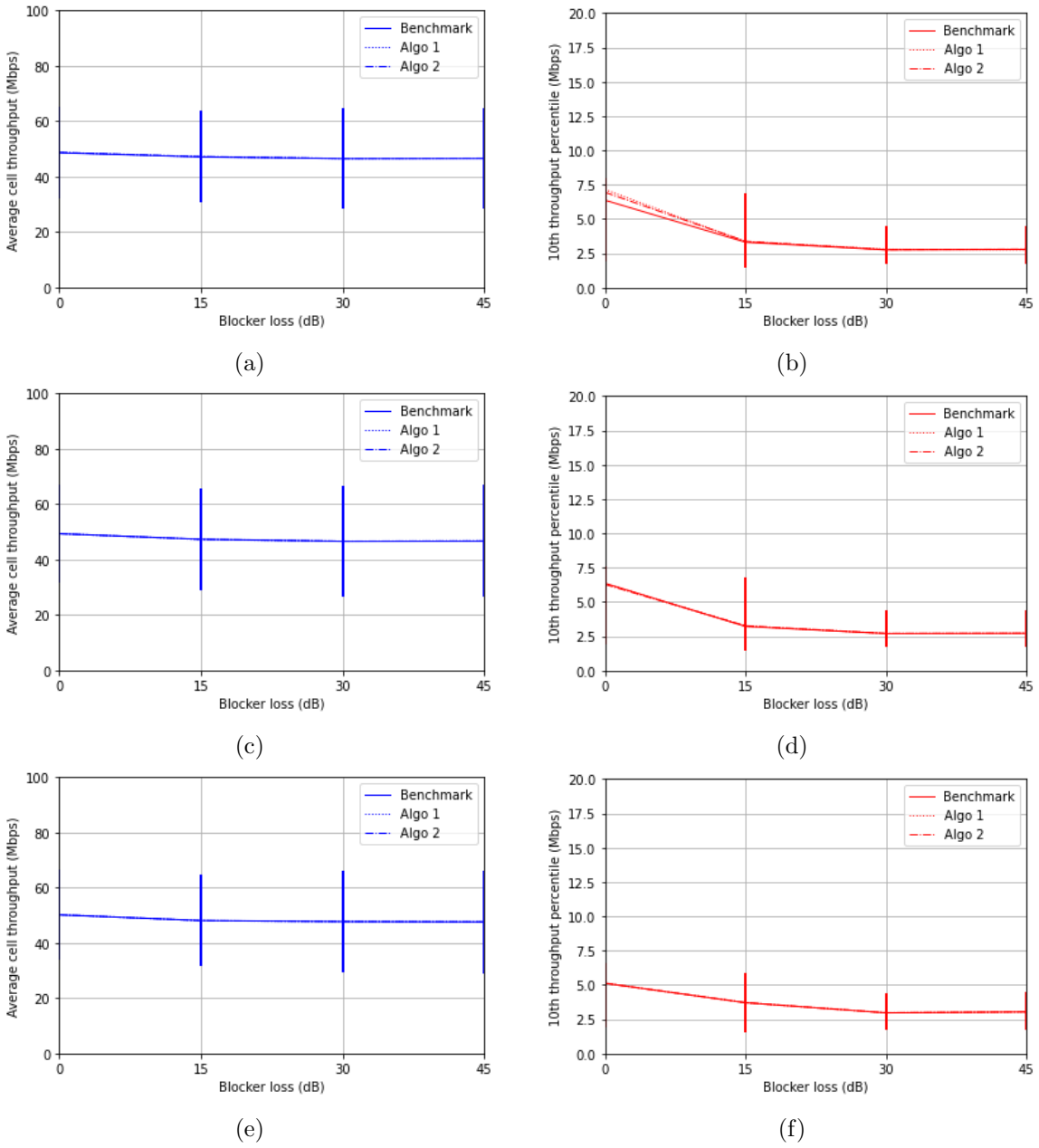


Figure A.5: MCSU: Performance achieved by the three algorithms for indoor users for RIS deployment position A in a-b, deployment position B in c-d, and for RIS deployment position C in e-f.